การศึกษาปริมาณรังสีและคุณภาพของภาพเอกซเรย์คอมพิวเตอร์บริเวณทรวงอกโดยใช้รังสีเอกซ์พลังงานค่าเดียวและสองพลังงาน ศึกษาในหุ่นจำลอง

นายธนินชัย จูตะวิริยะ

วิทยานิพนธ์นี้เป็นส่วนหนึ่งของการศึกษาตามหลักสูตรปริญญาวิทยาศาสตรมหาบัณฑิต
สาขาวิชาฉายาเวชศาสตร์ ภาควิชารังสีวิทยา
คณะแพทยศาสตร์ จุฬาลงกรณ์มหาวิทยาลัย
ปีการศึกษา 2560

RADIATION DOSE AND IMAGE QUALITY IN CHEST REGION
USING SINGLE- AND DUAL-ENERGY CT: PHANTOM STUDY

Mr. Taninchai Jutawiriya

A Thesis Submitted in Partial Fulfillment of the Requirements
for the Degree of Master of Science Program in Medical Imaging
Department of Radiology
Faculty of Medicine
Chulalongkorn University
Academic Year 2017

Thesis Title	RADIATION DOSE AND IMAGE QUALITY IN CHEST REGION USING SINGLE- AND DUAL-ENERGY CT: PHANTOM STUDY
By	Mr. Taninchai Jutawiriya
Field of Study	Medical Imaging
Thesis Advisor	Associate Professor Anchali Krisanachinda, Ph.D.

Accepted by the Faculty of Medicine, Chulalongkorn University in Partial Fulfillment of the Requirements for the Master's Degree

....Dean of the Faculty of Medicine

(Professor Suttipong Wacharasindhu, M.D.)

THESIS COMMITTEE

....Chairman

(Associate Professor Panruethai Trinvarat, M.D.)

....Thesis Advisor

(Associate Professor Anchali Krisanachinda, Ph.D.)

....Examiner

(Yothin Rakvongthai, Ph.D.)

....Examiner

(Associate Professor Kosuke Matsubara, Ph.D.)

....External Examiner

(Professor Franco Milano, Ph.D.)

ธนินชัย จูตะวิริยะ : การศึกษาปริมาณรังสีและคุณภาพของภาพเอกซเรย์คอมพิวเตอร์บริเวณทรวงอกโดยใช้รังสีเอกซ์พลังงานค่าเดียวและสองพลังงาน ศึกษาในหุ่นจำลอง (RADIATION DOSE AND IMAGE QUALITY IN CHEST REGION USING SINGLE- AND DUAL-ENERGY CT: PHANTOM STUDY) อ.ที่ปรึกษาวิทยานิพนธ์หลัก: รศ. ดร.อัญชลี กฤษณจินดา, 84 หน้า.

การตรวจพบก้อนในปอดในผู้ป่วยไทยมีเป็นจำนวนมาก ซึ่งจะต้องมีการติดตามอาการโดยการตรวจด้วยเอกซเรย์คอมพิวเตอร์บริเวณทรวงอกส่วนใหญ่จะใช้รังสีเอกซ์พลังงานเดียว ในปัจจุบันเครื่องเอกซเรย์คอมพิวเตอร์มีการพัฒนาให้มีการใช้พลังงานสองค่า วัตถุประสงค์ของงานวิจัยนี้คือการศึกษาปริมาณรังสีและคุณภาพของภาพเอกซเรย์คอมพิวเตอร์ระหว่างรังสีเอกซ์พลังงานเดียวและสองพลังงานโดยศึกษาในหุ่นจำลองบริเวณทรวงอก ภายในหุ่นจำลองจะใส่ก้อนเสมือนเนื้องอกจำนวน 5 ชิ้นซึ่งแต่ละชิ้นจะมีขนาดเส้นผ่านศูนย์กลางต่างกันโดยหุ่นจำลองจะถูกถ่ายภาพโดยเครื่องเอกซเรย์คอมพิวเตอร์ที่มีหลอดเอกซ์เรย์ 2 หลอด พารามิเตอร์ที่ใช้ในการถ่ายภาพประกอบด้วยโปรโตคอลรังสีเอกซ์ที่มีพลังงานค่าเดียวและสองค่าพลังงานซึ่งจะเปลี่ยนค่าความต่างศักย์ของหลอดเอกซเรย์ ปริมาณรังสีจะถูกคำนวณในรูปของค่าซีทีดีไอเชิงปริมาตร ($CTDI_{vol}$), ค่าดีแอลพี (DLP) และค่าปริมาณรังสียังผล (Effective dose) สำหรับคุณภาพของภาพจะถูกวัดในแง่ของสัญญาณรบกวนในภาพ (image noise), อัตราส่วนระหว่างความคมชัดต่อสัญญาณรบกวน (CNR) และความสามารถในการตรวจพบรอยโรค

ผลของงานวิจัยพบว่าค่าเฉลี่ยของปริมาณรังสีที่ความต่างศักย์ 120 เควีพี มีค่าสูงสุด ส่งผลให้สัญญาณรบกวนในภาพมีค่าต่ำกว่าภาพรังสีเอกซ์สองค่าพลังงาน สำหรับอัตราส่วนระหว่างความคมชัดต่อสัญญาณรบกวนของรังสีเอกซ์สองค่าพลังงานที่ 100/Sn150 เควีพี สูงกว่าค่าความต่างศักย์ที่ 120 เควีพี โดยที่ 120 เควีพี มีอัตราส่วนระหว่างความคมชัดต่อสัญญาณรบกวนสูงสุดในรังสีเอกซ์ที่มีพลังงานค่าเดียวและสูงกว่ารังสีเอกซ์ที่มีค่าพลังงานสองค่าที่ 80/Sn150 และ 90/Sn150 เควีพี สำหรับความสามารถในการตรวจหารอยโรค ในวินโดว์เนื้อเยื่อ (soft tissue window) พบว่าผู้สังเกตการณ์สามารถตรวจพบก้อนเสมือนรอยโรคที่รังสีเอกซ์มีสองพลังงานเหมือนกับค่าความต่างศักย์ค่าเดียวที่ 120 เควีพี สำหรับในวินโดว์ปอด (lung window) ผู้สังเกตการณ์ทุกคนสามารถตรวจพบก้อนจำนวน 5 ก้อนทั้งในรังสีเอกซ์พลังงานค่าเดียวและสองพลังงานซึ่งสอดคล้องกับโปรแกรมซีทีลังแคด (CT Lung CAD software) ซึ่งสามารถตรวจหาก้อนจำนวน 5 ก้อนเช่นกัน ดังนั้นการตรวจเอกซเรย์คอมพิวเตอร์แบบสองค่าพลังงานสามารถใช้ในการตรวจผู้ป่วยที่มีก้อนในปอดได้ เนื่องจากมีปริมาณรังสีน้อยกว่าการตรวจด้วยความต่างศักย์ค่าเดียวที่ 120 เควีพี ซึ่งส่วนใหญ่ใช้เป็นประจำในการตรวจทางคลินิก นอกจากนี้ความสามารถในการตรวจหารอยโรคของการตรวจเอกซเรย์คอมพิวเตอร์แบบสองค่าพลังงานเหมือนกับที่ 120 เควีพี ในขณะที่สัญญาณรบกวนในภาพของการตรวจเอกซเรย์คอมพิวเตอร์แบบสองค่าพลังงานมีค่าสูงกว่า 120 เควีพี ซึ่งจะมีผลต่อการแปลผลของรังสีแพทย์ ดังนั้นการตรวจเอกซเรย์คอมพิวเตอร์แบบสองค่าพลังงานสามารถถูกนำมาใช้ในการตรวจบริเวณทรวงอกได้ ขึ้นอยู่กับดุลยพินิจของรังสีแพทย์

ภาควิชา รังสีวิทยา	ลายมือชื่อนิสิต ....
สาขาวิชา ฉายาเวชศาสตร์	ลายมือชื่อ อ.ที่ปรึกษาหลัก ....
ปีการศึกษา 2560	

5974031930 : MAJOR MEDICAL IMAGING
KEYWORDS: DUAL-ENERGY CT / DUAL-SOURCE CT / CT CHEST / RADIATION DOSE / IMAGE QUALITY

TANINCHAI JUTAWIRIYA: RADIATION DOSE AND IMAGE QUALITY IN CHEST REGION USING SINGLE- AND DUAL-ENERGY CT: PHANTOM STUDY. ADVISOR: ASSOC. PROF. ANCHALI KRISANACHINDA, Ph.D., 84 pp.

Chest CT examinations are routinely performed by using single energy protocol (SE). As CT had been evolved by using dual energy protocol (DE), the patients with underlying lung nodules or pulmonary nodules will be followed up by CT examination several times. The purpose of this study is to study the radiation dose and image quality between single-energy CT (SECT) and dual-energy CT (DECT) protocols in chest phantom at King Chulalongkorn Memorial Hospital. The Lungman Kyoto Kagaku phantom inserted by five simulated lesions of various diameters was scanned by dual-source CT system (Somatom Force, Siemens Healthineers). The acquisition protocols consist of single-energy and dual-energy modes with varied tube potential. Radiation dose is determined in terms of CTDI volume ($CTDI_{vol}$), Dose Length Product (DLP) and effective dose. Image noise, CNR and lesion detectability are the image quality indicators in this study.

The results of this study show that the mean value of radiation dose in SE at 120 kVp was highest among all acquisition protocols, which results in lower image noise than DE. CNR of DE at 100/Sn150 kVp was greater than 120 kVp, all SE protocols, DE at 80/Sn150 and 90/Sn150. Regarding lesion detectability, in the soft tissue window, the simulated lesions were detected by the observers in dual energy mode as similar to in single-energy mode at 120 kVp. Moreover, in the lung window, all observers can detect the simulated lesions better than in soft tissue window, which results in five lesions were detected in both single- and dual- energy protocols, the same as CT lung CAD software could detect five simulated lesions. Therefore, DECT offers an alternative protocol for lung nodule detection because DECT offer lower radiation dose than SECT (120 kVp), clinical protocol in chest CT examination, in addition to lesion detectability DECT is similar to 120 kVp. In contrast, the image noise of DECT is higher than 120 kVp that affect the interpretation of radiologist. Therefore, DE protocols can be selected under the justification of qualified CT radiologist with the optimal protocol in chest CT examination.

Department:	Radiology	Student's Signature	....
Field of Study:	Medical Imaging	Advisor's Signature	....
Academic Year:	2017		

ACKNOWLEDGEMENTS

First of all, I would like to express my gratitude and deepest appreciation to Associate Professor Anchali Krisanachinda, Ph.D., Chair of Medical Imaging program, Department of Radiology, Faculty of Medicine, Chulalongkorn University, my advisor for her helpful, suggestion, guidance, supervision, constructive comments and polishing of the thesis to improve the readability and English expression, teaching of knowledge in Medical Imaging.

Second, I would like to deeply thank Associate Professor Panruethai Trinavarat, M.D., Department of Radiology, Faculty of Medicine, Chulalongkorn University, Chairman of thesis defense, Professor Franco Milano, Ph.D., University of Florence, Italy, external examiner, Associate Professor Kosuke Matsubara, Ph.D., Kanazawa University, Japan and Yothin Rakvongthai, Ph.D., Department of Radiology, Faculty of Medicine, Chulalongkorn University, examiners of thesis defense for their kind suggestion and constructive comments in this research.

Third, my gratitude is forwarded to Associate Professor Sivalee Suriyapee, Chief Physicist at Division of Radiation Oncology, Department of Radiology, Faculty of Medicine, Chulalongkorn University for her invaluable advices, constructive comments and teaching of knowledge in Medical Imaging.

Fourth, I would like to thank Pisit Chiyasak, M.D., Mr. Tiwa Jaiyai, Ms. Wanida Khunta, Department of Radiology, Bangkok Hospital for their kind evaluation on image quality in this research.

Fifth, I would like to truly thank Mrs. Petcharleeya Suwanpradit, Mrs. Walaiporn Suksancharoen and clinical staff at King Chulalongkorn Memorial Hospital for their kind support, guidance on CT scanner and suggestion in this research, shared the knowledge in Medical Imaging and facilitated to use CT scanner.

Sixth, I am greatly grateful all of the lecturers, medical physicists and staff in Medical Imaging Program, Faculty of Medicine, Chulalongkorn University for their suggestion and teaching of knowledge during the course of Medical Imaging.

Seventh, I gratefully appreciated the funding received from Bangkok Hospital for the opportunity to study in the master degree.

Furthermore, I would like to thank all of my friends in the class of Medical Imaging for their kindly support, suggestion either the research or the lecture.

Finally, I am extremely appreciated to my family for their invaluable encouragement, entirely care and understanding during the entire course of the study.

CONTENTS

Page

Page

LIST OF TABLES

LIST OF FIGURES

LIST OF ABBREVIATIONS

AEC	Automatic Exposure Control
CAD	Computer Aided Detection
CNR	Contrast to Noise Ratio
CT	Computed Tomography
CTDI	Computed Tomography Dose Index
$CTDI_w$	Weighted Computed Tomography Dose Index
$CTDI_{vol}$	Volume Computed Tomography Dose Index
DECT	Dual Energy Computed Tomography
DLP	Dose Length Product
DSCT	Dual Source Computed Tomography
E	Effective dose
FOV	Field Of View
HU	Hounsfield Unit
HVL	Half Value Layer
IAEA	International Atomic Energy Agency
K-factor	Conversion factor
kVp	Kilo-Voltage Peak
mA	MilliAmpere
mAs	MilliAmpere-Second
mGy	MilliGray
MPV	Mean Pixel Value
mSv	MilliSievert
MTF	Modulation Transfer Function
PMMA	Polymethyl methacrylate
QC	Quality Control
ROI	Region Of Interest
SAFIRE	Sinogram Affirmed Iterative Reconstruction
SD	Standard Deviation
SECT	Single Energy Computed Tomography
Sn	Stannous - tin
SPN	Solitary Pulmonary Nodule
TCM	Tube Current Modulation

CHAPTER I

INTRODUCTION

1.1 Background and rationale

At present, the application of computed tomography (CT) is increasing in medical imaging due to its ability in displaying the anatomy and pathology of internal organs for the clinical diagnosis. In CT imaging, the materials of different compositions can be represented by the same or very similar CT numbers. A simple example is the difficulty in differentiating between calcified plaques and iodine-filled in blood vessel. Therefore, CT has been developed to be more efficient through the use of dual energy CT [1], which could differentiate calcification from iodinated contrast media in bloods vessel and soft tissue plaques from fatty tissue.

Dual-energy CT refers to the system producing two photon spectra that can be defined as the use of attenuation measurements by different energy spectra. An increased interest in DE scanning, driven by three types of dual-energy CT scanners, differ in the technique to acquire high- and low-energy CT datasets: a dual- source dual-energy scanner, a single-source dual-energy scanner with fast kilo-voltage switching (rapid alternation between high and low kilo-voltage settings), and a single-source dual-energy scanner with dual detector layers [1].

Dual-energy CT offers advantages in several clinical applications such as: identify renal calculi, subtract bone and calcification in CT angiogram, generate virtual non-contrast dataset by subtracting iodine, assess myocardial perfusion and visualize lung perfusion or ventilation, detect calcification in pulmonary nodules [1-4].

Solitary pulmonary nodule, SPN, can be detected incidentally on screening chest x-rays or chest CT examination. It is defined as a spherically-shape lesion that measured up to 3 cm in diameter (larger than that is considered mass) and is entirely surrounded by lung tissue. Diagnosis of lung nodule can be made by a lung biopsy. Tissue obtained by bronchoscopic biopsy is commonly used for diagnosis for central lesion. CT guided percutaneous transthoracic needle biopsies have also been proven to be very helpful in the diagnosis of SPN [5].

There are a lot of patients with underlying lung nodules or pulmonary nodules each year, in Thailand. These patients will be followed up by the CT examination several times. Hence, the patients will obtain a higher cumulative radiation dose that may contribute to a higher risk of development in the future.

Both the radiation dose and the image quality characteristic in CT examination are controlled by the specific imaging protocol selected for each patient. The protocol is created from a complex combination of many adjustable imaging factor or parameters for each procedure. The objective for each imaging procedure is to adjust the image characteristics to provide the required visualization of anatomical structures, signs of pathology and limit the radiation dose to produce the necessary image quality.

Furthermore, many local and global professional organizations are aware of the patients' radiation dose as the CT examination rate is increasing. The issue of radiation dose reduction is currently drawing pervasive attention. As a result, several radiation dose reduction techniques, such as automatic exposure control (AEC) or tube current modulation (TCM), tube voltage reduction, iterative reconstruction and utilization of dual-energy technique while attempt to maintain diagnostic image quality had been reported and commercially available.

Chest CT examination is performed traditionally by using single energy protocol, 120 kVp, while, the study of thorax region with dual-energy CT protocol is rare. Hence, the dual-energy CT protocol is interesting in terms of radiation dose and image quality. Chest region is composed of several internal organs such as breast and lung which are sensitive to radiation and the effect of radiation to such the organs are directly proportional to radiation dose. As a result, chest CT examination should provide the patients with low radiation dose. On the other hand, the low radiation dose would bring insufficient image quality for interpretation. Therefore, the protocol of chest DECT examination should be obtained for the optimization purpose.

1.2 Research objective

To study the radiation dose and image quality between single-energy CT, as a standard chest scan, and dual-energy protocol in chest phantom using CT chest protocol of King Chulalongkorn Memorial Hospital.

1.3 Definition

Dual-energy CT	The new technique of CT protocol, consist of two CT datasets with different photon spectra, was designed by many vendors that have different technical approach. It can characterize urinary stones, generate virtual non-contrast images from post-contrast enhanced scans.

CHAPTER II
REVIEW OF RELATED LITERATURE

2.1 Theory

2.1.1 Computed Tomography (CT) [6]

A computed tomography is a diagnostic imaging procedure that uses x-rays to generate cross-sectional images or slices of the body. Cross-sectional images are reconstructed from the measurement of attenuation coefficient of x-ray beam in the volume of the object. CT is based on the fundamental principle that the density of the tissues passed by the x-ray beam can be measured from the calculation of the attenuation coefficient.

Early CT scanner acquired images one single slice at a time (sequential scanning). However, since the 1980s CT has been developed to continuously rotating x-ray tube and detector system, made by a slip-ring technology for electrical power supply and data acquisition, with a fan beam covering the total patient cross-section and corresponding to detector array, of scintillation detector.

In 1989, CT technology was developed to spiral or helical CT, the x-ray tube rotates continuously in one direction the patient table is moved with constant velocity along his body direction (z-axis) through the x-ray beam; this results in a spiral track of the focal spot around the patient and accordingly in a spiral data set as shown in Figure 2.1. In place of acquiring the data from one slice at a time, the information can be obtained as a continuous volume of contiguous slices. This method allows larger anatomical regions of the body to be imaged in a single breath hold, therefore reducing the artifacts causes by patient movement. It helps to faster scanning, increases the probability in diagnostic with the patient who unconscious or unable to cooperate with the examinations.

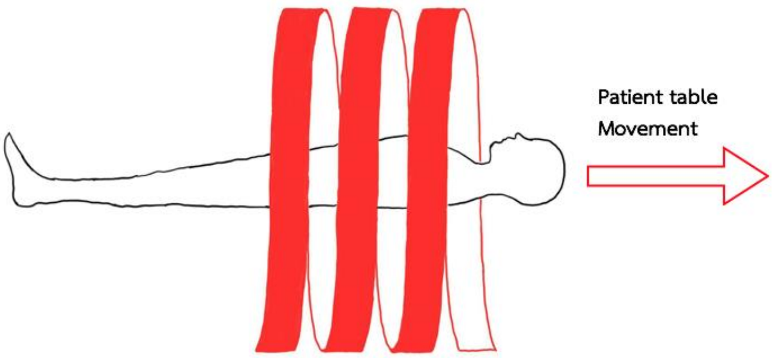

Figure 2.1 Single-slice helical CT [6].

In 1992, CT scanners were launched to the multi-detector or multi-slice scanners utilize the principle of the helical scanners but incorporate multiple rows of the detector rings. Consequently, they can obtain multiple slices in one tube rotation as shown in Figure 2.2.

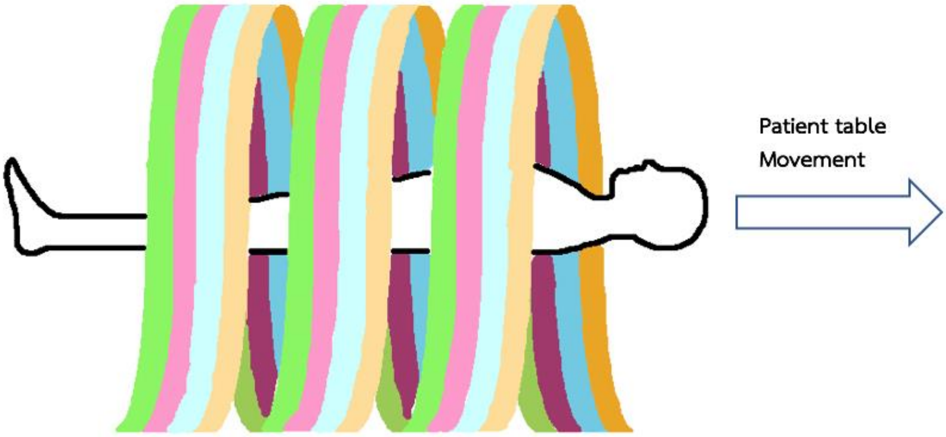

Figure 2.2 Multi-slice helical CT [6].

2.1.2 Dual-energy CT

Dual energy CT or DECT produced two spectra of photons, therefore DECT is sometimes referred to as spectral CT. The x-ray sources consist of x-ray tubes with rotating anodes that have poly-chromatic spectra of bremsstrahlung superimposed with characteristic lines of the tungsten material of the anode. The maximum energy of the photons is defined by the voltage, whereas the mean energies are significantly lower and their differences are smaller than one may expect. The settings of 80 and 140 kVp are commonly used because they provide the maximum difference and least overlap between the spectra with standard tubes as illustrated in Figure 2.3. [7].

There are three DECT platforms. First: dual sources, dual energies CT utilize two X-ray tubes and two sets of detectors to obtain simultaneous dual energy acquisition and data processing. Second: single source, dual energies CT uses a single X-ray tube that rapidly alternates between low and high energies (fast-switching) and a single set of detector that quickly registers information from both energies. Third: in detector based spectral CT, a single X-ray tube with full dose modulation capabilities is paired with a set of detectors made of two layers (sandwich detector) that simultaneously detects two energy levels [1, 7].

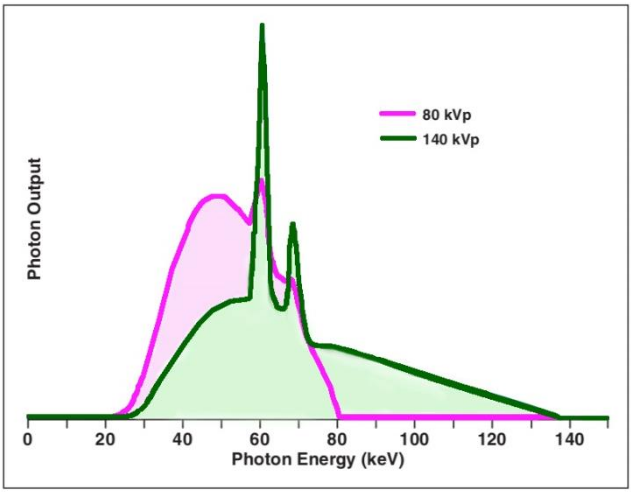

Figure 2.3 Combination of 80 and 140 kVp are used for sequential acquisition. Overlap between both spectra is quite broad [7].

2.1.3 Dual-source CT

Dual-source CT is a system which two x-ray sources and two corresponding detector systems are mounted on the same gantry, positioned orthogonally to one another. Each x-ray tube operates at a different voltage, one at lower voltage, and the other one at higher voltage to provide maximum difference of their spectra. The latter offers least spectra overlap. The tubes rotate simultaneously in a fixed position relative to each other, thus avoiding temporal differences in projection sampling. Detector A covers the entire scan field-of-view with a diameter of 50 cm, detector B covers the field of view over limited to 26, 33 or 35 cm, depending on the specific scanner model as shown in Figure 2.4 [7, 8]. After scanning, dual-energy mode, 3 data sets of the image will be acquired during a single acquisition:

1. Raw data image from low energy.
2. Raw data image from high energy.
3. Fast DE series image from composite ratio of image data from low energy and high energy.

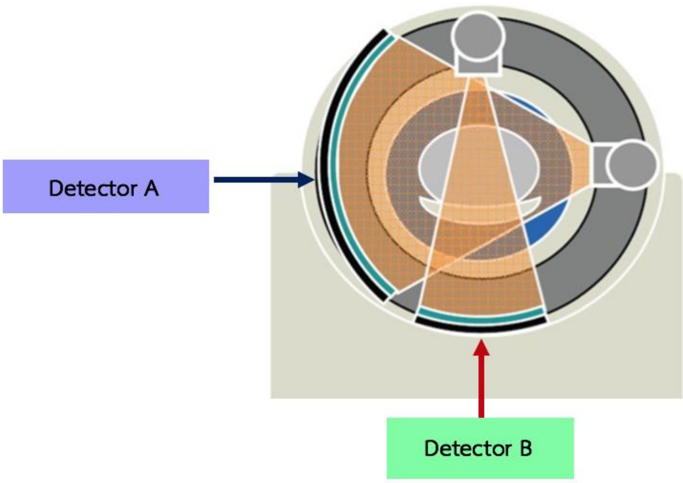

Figure 2.4 Dual-source CT [8].

Images reconstructed from each of the tube-detector pairs are used to perform material decomposition analyses in the image domain. Because each tube is operated at different tube potentials and different tube current values, the noise levels in the respective images are adjustable. Because both tubes are simultaneously energized, scattered radiation came from one tube may be detected by the detector for the other tube, and vice versa. Second generation of dual source CT scanners, tin (Sn) filter is used to eliminate low energy from high-energy spectrum and decrease overlap of spectrum between low- and high-energy. Therefore, high tube voltage merged with filter offer improvement in spectral contrast. As the body consists of different photon attenuation materials depended on tissue composition and photon energy closed to K-edge of the material, dual-energy can be used to distinguish material composition by image acquisition at two different photon energies, and increased signal-to-noise ratio in the material-specific images.

2.1.4 Hounsfield unit or CT number [6]

In CT images, each pixel is determined a numerical value (CT number), which is the average of the attenuation values contained within the voxel. This number is compared to the attenuation value of water as following in equation 2.1 and displayed in term of Hounsfield unit (HU).

$$HU = \frac{\mu_{tissue} - \mu_{water}}{\mu_{water}} \times 1000 \quad , \qquad (2.1)$$

where μ_{tissue} is the linear attenuation coefficient of tissue.

μ_{water} is the linear attenuation coefficient of water.

The CT number of water is determined as an attenuation value (HU) of zero. The wide range of CT numbers is 2000 HU even though some modern scanners have a greater range of HU up to 4000. Each number supersede a shade of grey scale with white (+1000) and black (-1000) at either end of the spectrum. The CT number of each tissue is shown in Figure 2.5.

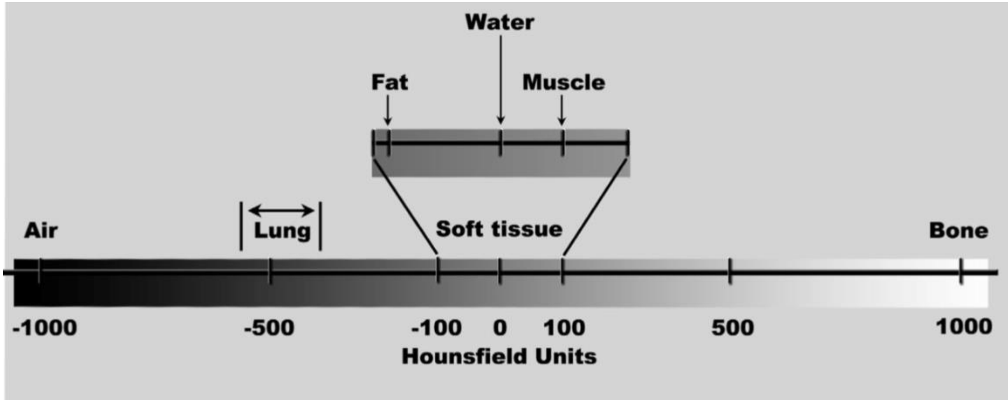

Figure 2.5 The Hounsfield unit in each tissue [9].

2.1.5 Radiation dose [10]

2.1.5.1 Computed Tomography Dose Index (CTDI) [10]

The dosimetric quantity in CT is Computed Tomography Dose Index (CTDI) measured in cylindrical phantoms. CTDI represents average dose along the z direction, from a series of contiguous irradiation. It is measured from one axial CT scan or one rotation of x-ray tube and estimates the average dose within the central region of a scan volume. For MDCT, CTDI is calculated by dividing of the integrated of absorbed dose by the nominal total beam collimation as shown in equation 2.2.

$$\mathrm{CTDI} = \frac{1}{NT}\int_{-\infty}^{\infty} D(z)\, dz \quad , \tag{2.2}$$

where D(z) denotes the radiation dose profile along z direction

N denotes the number of acquire slices per single axial scan

T denotes the nominal scan width of acquire slice

2.1.5.1.1 CTDI100 (C_{100}) [10]

The CTDI_{100} represent the accumulated multiple scan dose at the center of 100 mm scan and underestimates the accumulated dose for longer scan lengths. It requires integration of the radiation dose profile from a single axial scan over specific integration limits and the integration limits are ± 50 mm, which corresponds to the 100 mm length of pencil ionization chamber. The

$CTDI_{100}$ is calculated by the integral of air kerma along ionization chamber divided by nominal slice thickness as shown in equation 2.3.

$$CTDI_{100} = \frac{1}{NT}\int_{-50\text{ mm}}^{50\text{ mm}} D(z)\, dz \;, \tag{2.3}$$

where D(z) denotes the radiation dose profile along z direction

NT denotes nominal width of irradiation beam

The use of single, consistent integration limit avoided the problem of dose overestimation for narrow slice widths. The $CTDI_{100}$ is received by using 100 mm long, 3 cc active volume CT pencil ionization chamber and the two standard PMMA phantoms; head (16 cm diameter) and body (32 cm diameter). The measurement of $CTDI_{100}$ must be performed with the stationary patient table.

2.1.5.1.2 Weighted CT Dose Index ($CTDI_w$, C_w) [10]

The $CTDI_w$ represents the CTDI varies across the field of view (FOV). Typically, the CTDI is used a factor or two time at the surface than at the center of the FOV. The C_w is defined as the summation of one-third of the $CTDI_{100}$ measured at the center of the phantom and two-third of the $CTDI_{100}$ measured at the periphery of the phantom as shown in the equation 2.4.

$$CTDI_w = \frac{1}{3} CTDI_{100,center} + \frac{2}{3} CTDI_{100,peripheral} \tag{2.4}$$

2.1.5.1.3 Volume CT Dose Index ($CTDI_{vol}$, C_{vol}) [10]

The $CTDI_{vol}$ represents the average absorbed radiation dose within the scan volume for a standardized (PMMA) phantom, over the x, y and z axis, for a specific exam protocol. It is the most commonly cited index for modern MDCT equipment and provides a single CT dose parameter, based on a directly and easily measured quantity. The SI unit is milliGray (mGy). Its value may be displayed on the console of modern CT scanners. $CTDI_{vol}$ is necessary to take into account any gaps or overlaps between the x-ray beams from contiguous rotations of the x-ray tube. $CTDI_{vol}$ is defined as:

$$CTDI_{vol} = \frac{N \times T}{I} \times CTDI_w \;, \tag{2.5}$$

where I denotes the table increment per axial scan (mm)

Since pitch is defined as the ratio of the table travel per rotation (I) to the total nominal beam width (N x T) as following:

$$\text{Pitch} = \frac{I}{N \times T} \tag{2.6}$$

Therefore, $CTDI_{vol}$ can be expressed as

$$CTDI_{vol} = \frac{1}{\text{pitch}} \times CTDI_{w} \tag{2.7}$$

While $CTDI_{vol}$ estimates the average radiation dose within the irradiated volume for an object of similar with attenuation of the PMMA phantom, it does not represent the average dose for objects of substantially different size, shape, or attenuation. Moreover, it does not indicate the total energy deposited to the scan volume because it is independent to the length of the scan.

2.1.5.2 Dose Length Product (DLP) [10]

The DLP represents the overall dose delivered by a given scan protocol. It is a measure of CT tube radiation output/exposure. It is related to $CTDI_{vol}$ but $CTDI_{vol}$ represent the dose through a slice of an appropriate phantom. DLP accounts for the length of radiation output along the z direction (the long axis of the patient) as shown in equation 2.8. This value is expressed in milliGray*centimeters (mGy.cm)

$$DLP = CTDI_{vol} \times \text{scan length} \tag{2.8}$$

The DLP reflects the total energy absorbed (and thus the potential biological effect) attributable to the complete scan acquisition. Thus, an abdomen-only CT exam might have the same $CTDI_{vol}$ as an abdomen/pelvis CT exam, but the latter exam would have a greater DLP, proportional to the greater z-extent of the scan volume.

In helical CT, data interpolation between two points must be performed for all projection angles. Thus, the images at the very beginning and end of a helical scan require data from z-axis projections beyond the defined “scan” boundaries (i.e., the beginning and end of the anatomic range over which images are desired). This increase in DLP due to the additional rotation required for the helical interpolation algorithm is often referred to “over ranging”. For MDCT scanners, the number of additional rotations is strongly pitch dependent, with a typical increase in irradiation length of 1.5 times the total nominal beam width.

The implication of over ranging with regard to the DLP depends on the length of the imaged body region. For helical scans that are short relative to the total beam width, the dose efficiency (with regard to over ranging) will decrease. For the same anatomic coverage, it is generally more dose efficient to use a single helical scan than multiple helical scans.

2.1.5.3 Effective dose (E) [10]

Effective dose is a dose descriptor that reflects the difference in biologic sensitivity. It is a single dose parameter that reflects the risk of a non- uniform exposure in terms of an equivalent whole-body exposure. The unit of effective dose, in diagnostic radiology, is milliSievert (mSv).

The concept of effective dose is designed for radiation protection of occupationally exposed personnel. It reflects radiation detriment averaged over age and gender, and its application has limitation when applied to medical populations. The effective dose describes the relative "whole-body" dose for a particular exam and scanner but is not the dose for any one individual. Effective dose is used to optimize exam and to compare risks between proposed exams. It is a broad measure of risk.

The most direct method to estimate doses to the patients who undergoing CT examination is to measure organ doses in patient-like phantoms. Another method is by calculation using Monte Carlo methods follow the paths of a large number of x-ray as they interact with a virtual phantom. The resultant information is the absorbed dose to a specified tissue, which may be used to predict the biological consequences to that (single) tissue. CT examinations, however, irradiate multiple tissues having different radiation sensitivities. The effective dose takes into account how much radiation is received by an individual tissue, as well as the tissue's relative radiation sensitivity

Effective dose values calculated from the National Radiological Protection Board (NRPB) Monte Carlo organ coefficients were compared to DLP values for the corresponding clinical exams to determine a set of coefficients, K, where the values of K are depended on the region of the body was scanned (head, neck, chest, abdomen, and pelvis) as shown in Table 2.1. Using this methodology, the effective dose can be calculated as equation 2.9.

$$\text{Effective dose} = \text{DLP} \times \text{K} \quad (2.9)$$

Table 2.1 Conversion factor to normalize effective dose per Dose Length Product (DLP) for pediatrics and adults' patients of various ages over various body regions.

Region body	K-factor (mSv/mGy.cm) [10]				
	0-year-old	1-years-old	5-years-old	10-years-old	Adults
Head	0.0110	0.0067	0.0040	0.0032	0.0021
Neck	0.0170	0.0120	0.0110	0.0079	0.0059
Head & Neck	0.0130	0.0085	0.0057	0.0042	0.0031
Chest	0.0390	0.0260	0.0180	0.0130	0.0140
Abdomen & Pelvis	0.0490	0.0300	0.0200	0.0150	0.0150
Trunk	0.0440	0.0280	0.0190	0.0140	0.0150

2.1.6 Image quality

In CT scanning, the image quality can be described as image noise, spatial resolution and contrast resolution.

2.1.6.1 Image noise [11]

In CT, x-rays contribute to detector measurement, the image noise is associated with the numbers of x-ray photons with the detector as quantum noise. Since photon statistics follow the Poisson distribution, quantum noise is proportional to N, number of the x-ray photon, and inversely proportional to the square root of the exposure to the detector that have contributed to the reconstructed image.

The parameters influenced the image noise are as following:

- Tube voltage (kVp): Increasing of kVp contributes to increase the number of x-rays penetrating the patient and reaching the detectors. Hence, increasing the kVp reduces image noise but can (slightly) also reduce subject contrast.
- Tube current (mA): Changing the mA value cause to change the beam intensity and the number of x-rays. Such as, doubling the mA value will double the beam intensity and the number of x-rays detected by each measurement. So, the image noise decreases.
- Tube rotation time: Changing the scan time lead to change the duration of each measurement and affect to the number of x-rays photon. Because tube current and rotation time similarly affect to image noise and patient radiation dose, they are usually considered together as mA·s, or mAs.

- Slice thickness: Changing the thickness will change the beam width entering each detector and number of x-rays photon approximately proportionally. For example, compared with a slice thickness of 5 mm, a thickness of 10 mm approximately doubles the number of x-rays entering each detector.

Image noise in CT appears as fluctuations in CT numbers, a measurement of image noise is a measurement of these fluctuations, and such a measurement can be made using regions of interest (ROIs) on a scan of a uniform phantom. A statistical ROI function allows users to place a rectangular or oval ROI on the image, within which is calculated the average and standard deviation (SD) of the CT numbers for the enclosed pixels. The SD indicates the magnitude of random fluctuations in the CT number. Therefore, the larger of SD, the image noise is higher.

2.1.6.2 Spatial resolution [12]

Spatial resolution is the ability to distinguish small objects on the image. The method to measure spatial resolution of the image is high contrast test objects where signal to noise ratio level is high and does not affect recognition. It can be specified in term of spatial frequency, line pairs per cm (lp/cm). Whereas, the modulation transfer function (MTF) uses to measure imaging system transfer the information from the object to the image. The unit of MTF is expressed in percent.

CT resolution is generally limited by the size of the detector or aperture size and the spacing of the detector, used to reconstruct the image. The aperture is approximately equal to the detector width.

2.1.6.3 Contrast resolution

Contrast resolution is the ability to distinguish between differences in intensity in the image. Contrast resolution is known as low contrast resolution and tissue resolution. CT can display tissue image that varies only slightly in atomic number and density. Most soft tissue has similar atomic number or densities. Contrast resolution describes the CT systems ability to discriminate between two or more anatomical structures, have attenuate nearly the same amount of x-ray photons. It is a difficult quantity to define contrast resolution, because it depends on the human observer as much as the quality of the actual image. Contrast resolution is limited by noise, as noise is increasing, contrast resolution will decrease [13].

Generator power is necessary for low contrast examinations. Low image noise requires high tube current (mA), particularly when coupled with fast speed rotation and narrow slice acquisition. Due to, fast speed rotation decreases movement artifacts, thin slice thickness contributes to improve spatial resolution and also decrease partial volume effects [8].

2.1.7 Automatic Exposure Control (AEC) [14]

Automatic exposure control could be defined as a CT technique that performs automatic modulation of tube current in the x, y plane (angular modulation), or along the scanning direction, z-axis, (longitudinal modulation), or both (combined modulation). The modification is done according to each patient's size, shape and attenuation of body parts being scanned. The required image quality level must be selected and the system can adjust the tube current to obtain the predetermined image quality with improved radiation efficiency. AEC system (angular modulation) can in most cases reduce radiation dose by typically between 10-50%, without any deterioration of the image quality. In the shoulder region is even more than 50% dose reduction possible, because of big differences in attenuation. However, for large patients the radiation dose can increase to preserve the specified image quality.

2.1.7.1 Angular modulation [14]

With a fixed tube current technique, the X-ray tube rotates around the patient continuously emitting X-rays with constant fluence. In angular (rotational) modulation technique the tube current is adjusted for each projection angle to the size, shape and attenuation of the patient in order to minimize X-rays in beam projection angles (in the x- and y-axes) that are associated with less beam attenuation and consequently contribute less to the overall image noise. For example, in anatomy that is highly asymmetric such as the shoulders and pelvis, the X-ray beams are much less attenuated in the anterior-posterior direction compared with the lateral direction and hence is associated with less noise as shown in Figure 2.6. For that reason, angular modulation technique reduces unneeded radiation in the anterior-posterior projection without any obvious degradation of the image quality. In regions where the patient is more circular and homogenous, such as the head, less modulation will occur.

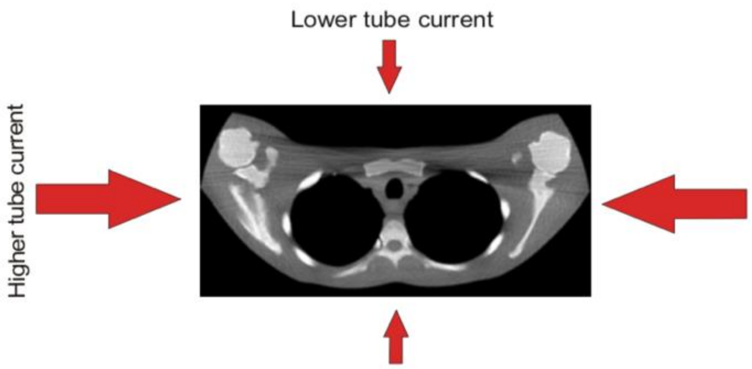

Figure 2.6 Principle of angular modulation technique; in the shoulder region it is possible to reduce the tube current in the anterior-posterior direction compared with the lateral direction, which is the thickest cross section and has an amount of bony material that attenuates the X-rays [14].

In asymmetric regions of the body, e.g. the shoulders, where the lateral scan range goes through the thickest cross section and has a higher than usual amount of bony material, starvation (streaking) artifacts can arise. This artifact is due to insufficient of photons in the attenuation measurements, in the lateral direction. Angular modulation tries to diminish the variation in uncertainty of attenuation measurements by increasing the tube current in lateral projection angles and reducing where the attenuation is lower. This has the effect that the noise is more uniform across the image and starvation artifacts will be reduced.

2.1.7.2 Longitudinal (z-axis) modulation [14]

When a fixed tube current technique is used, the images are acquired at a constant tube current value along the scanning direction (z-axis), independent of patient size or local attenuation. With longitudinal modulation technique, the tube current is adjusted along the scanning direction (z- axis) of the patient, grounded on the size, shape and attenuation of the anatomic region being scanned as illustrated in Figure 2.7. The purpose of longitudinal modulation technique is to produce similar noise in all images independent of patient size and anatomy. The aim is also to reduce the variation in image quality from patient to patient. Consequently, the operator must select a required level of image quality as an input to the AEC algorithm. The methods are different between various manufacturers. But irrespective of type, the longitudinal modulation technique uses a single localizer radiograph to determine the tube current required to produce images with required level of image noise.

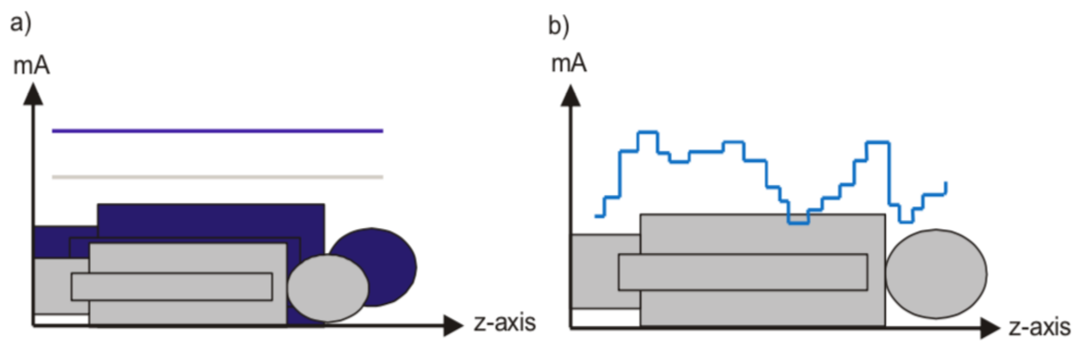

Figure 2.7 Illustrations of longitudinal modulation a) Lower mA is used for a smaller patient. b) lower mA is used where the attenuation is low along the scanning direction, e.g. lung region [14].

2.1.7.3 Combined modulation [14]

Combined modulation technique is a simultaneous combination of angular and longitudinal (x-, y-, and z-axis) tube current modulation, i.e. this technique modulates the tube current both during each gantry rotation and for each slice position as shown in Figure 2.8. The required level of image quality must be specified. Combined modulation technique is the most extensive approach to CT dose reduction, since the X-ray dose is adjusted in accordance with the patient attenuation in three dimensions.

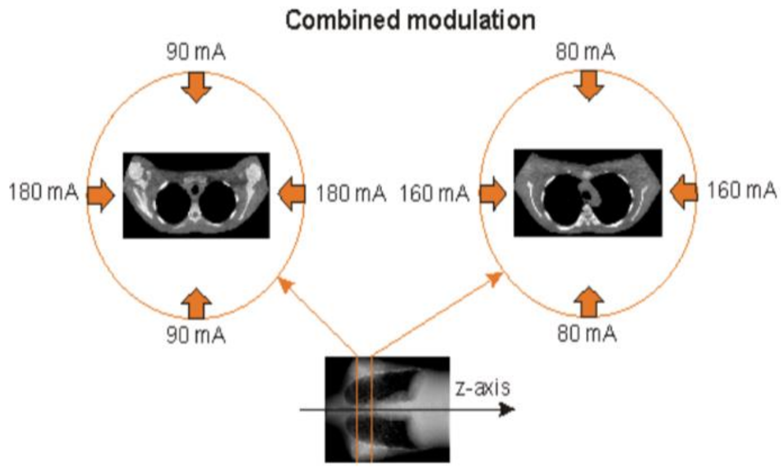

Figure 2.8 Combined modulation, the tube current is adjusted during each gantry rotation (in x, y axes) and adjusted along the scanning direction (z- axis) of the patient according to the size, shape and attenuation of body region being scanned. Therefore, different slice positions obtained different tube currents according to direction (z-axis) and projection angles during the gantry rotation [14].

2.2 Review of related literature

The measurement of radiation dose and image quality in Dual energy CT on Dual source CT scanner was reported as the followings:

Kosuke Matsubara, Tadanori Takata, Masanao Kobayashi, et al [15]. reported 'Tube Current Modulation Between Single- and Dual- Energy CT with a Second-Generation Dual Source Scanner: Radiation Dose and Image Quality'. The objectives of the study were to compare the effects of tube current modulation between single- and dual-energy CT with a second-generation dual-source scanner and to compare radiation dose and image quality in single- and dual-energy, by using elliptical polymethyl methacrylate phantoms, represent slim and large patients, scanned by 120, 80/Sn140 and 100/Sn140 kVp with tube current modulation (TCM). Radiation dose was measured by using solid state detector, inserted in the phantom. Image quality was determined in term of image noise. The results show that at 80/Sn140 kVp, for both slim and large phantoms, obtained lower radiation dose and higher image noise than at 120 kVp and 100/Sn140 kVp at all quality reference tube current–time settings. For the large phantom scanned with 100/Sn140 kV, the system responded with an alert that the peak exposure demand for TCM exceeded the system limit and was changed the tube current–time setting automatically.

Jan C. Schenzel, Wieland H. Sommer, Klement Neumaier, et al [16]. reported 'dual energy CT of the chest, How about dose?'. The objectives of this study were to assess dose and image noise of two different dual energy CT setting with reference to a standard chest scan and to compare image noise and contrast to noise ratio. Anthropomorphic Alderson Rando phantom was assembled with 58-TLD that allocated to every organ in several slices in the scan range and inserted syringes that mixture of contrast material and saline. Its chest was scanned by using three different protocols, such as 80/140, 100/Sn140 and 120 kVp, on dual source CT. Radiation dose was evaluated in term of effective dose, calculated from the TLD measurement and specific conversion coefficients. Image noise was measured by drawing ROIs at different positions in a homogenous area of the mediastinum. CNR was evaluated in two ways such as general CNR, quotient of the mean pixel value of contrast material in the syringe and standard deviation (S.D.) in images of dual energy and in 120 kVp images, and spectral contrast, differentiate between CT number in the center of the iodine syringe divided by the background noise. The results indicated that effective dose of 120 kVp was higher with slightly lower image noise than 80/140. In contrast, effective dose from DLP and TLDs of 100/Sn140 kVp was higher and lower than 120 kVp respectively but image noise was higher than 120 kVp. Regarding CNR, at 100/Sn140 kVp provides a smaller CNRspectral contrast than 140/80 kVp. Due to the larger overlap of the spectra and higher mean energy which results in a loss of photoelectric effect. The transmission of photon increases benefit for examination in obese patients whereas, 120 kVp provide CNR as equal to 80/140 kVp.

From both literature reviews, SE (120 kVp) offer higher radiation dose and better image quality than DECT, performed in second generation of DSCT. At King Chulalongkorn Memorial Hospital DSCT, third generation is different in tube potential in DE from second generation. The study of radiation dose and image quality in DE, third generation of DSCT should be performed.

CHAPTER III
RESEARCH METHODOLOGY

3.1 Research design

This study is observational descriptive study.

3.2 Research design model

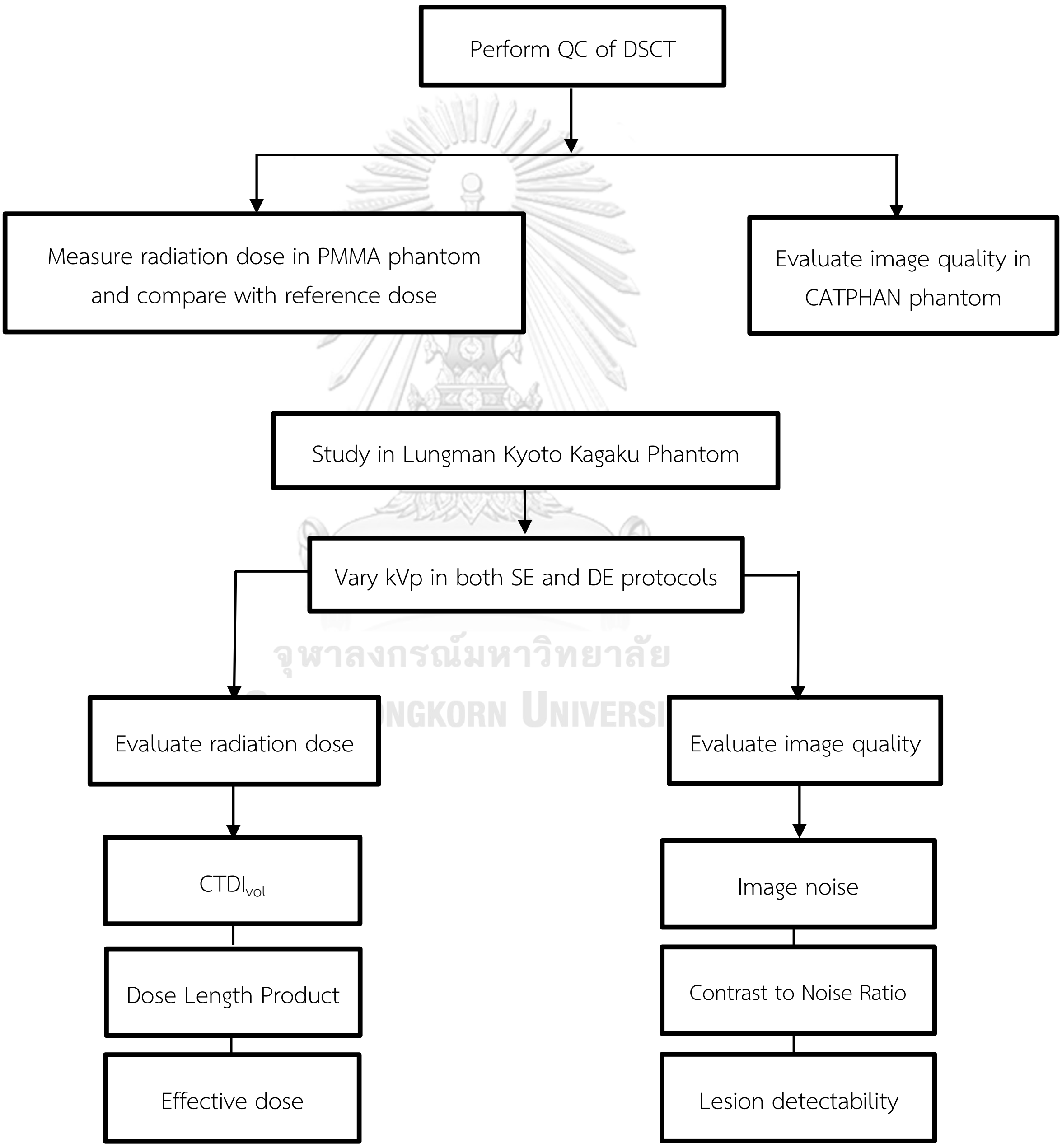

3.3 Conceptual framework

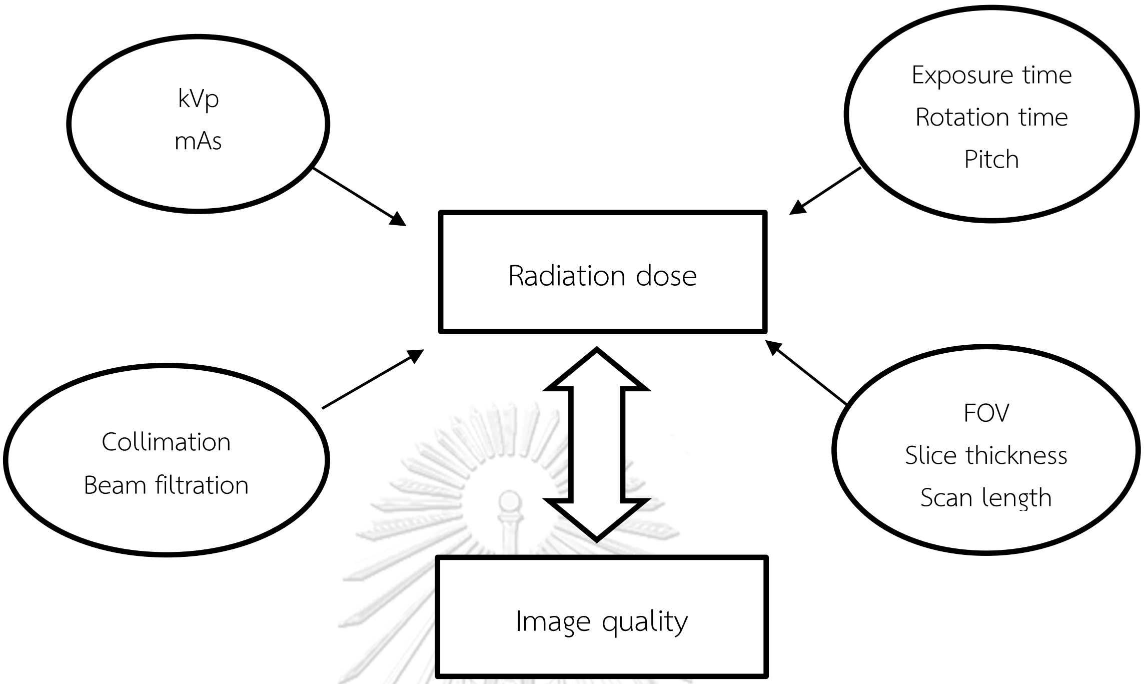

3.4 Research question

What are radiation dose and image quality of dual – energy in chest phantom in comparison to single-energy using dual – source CT (Somatom Definition Force, Siemens)?

3.5 Materials

3.5.1 CT scanner, Somatom® Definition Force, Siemens

Figure 3.1 Dual-source CT, Somatom® Definition Force, Siemens.

This CT scanner model Somatom Definition Force, the range of kVp is 70-150, number of tube is 2, number of detector is 2 stellar infinity® detector with 3D anti-scatter collimator, tin filter is implemented in the high voltage tube, 192 x 0.6 mm detector configuration (physical z-coverage of 96 x 0.6 mm, with a z-flying focal spot), full field of view of 50 cm, gantry rotation time up to 0.25 seconds, 240 kW for generator power, table loading up to 307 kg manufactured by Siemens Healthcare [17] as shown in Figure 3.1. This scanner is the third generation of dual source CT, with an AEC system (CAREdose4D) to automatically modulate tube current. The system was installed at the Department of Radiology, King Chulalongkorn Memorial Hospital in 2015.

3.5.2 Lungman chest phantom

Lungman chest phantom (Kyoto Kagaku Co.Ltd.) is composed and constructed to mimic standard human chest. The inner components of the phantom consist of mediastinum, pulmonary vasculature and abdomen block as depicted in Figure 3.2. The phantom is inserted by simulated lesions in lung field. The x-ray properties of the soft tissue substitute material and synthetic bone are similar to the human tissues. The phantom is applicable for the both CT scanning and plain radiograph. The phantom size is 43 x 40x 48H cm, chest girth 94 cm as standard man of 80 kg [18].

Figure 3.2 Lungman chest phantom.

3.5.3 The simulated sphere lesions

Five sizes of simulated sphere lesions at different diameter of 3, 5, 8, 10 and 12 mm were attached in lung field of Lungman chest phantom as illustrated in Figure 3.3. The lesions were made of polyurethane and hydroxyapatite with CT number of 100 HU [18].

Figure 3.3 Simulated sphere lung lesions of 3, 5, 8, 10, 12 mm in diameter.

3.5.4 PMMA phantom

Two cylindrical phantoms simulated head and body have been used to perform quality control of CT system. Both phantoms were made of polymethyl methacrylate (PMMA). The head phantom is 16 cm in diameter nested within the body phantom of 32 cm in diameter. Both phantoms contain 5 holes, one at the center and four at the peripheries, at 1 cm from the phantom edge. All holes were inserted by a pencil ion chamber and for acrylic rods during radiation dose measurement at all hole position [19] as shown in Figure 3.4.

Figure 3.4 PMMA phantoms of 16, 32 cm in diameter.

3.5.5 CATPHAN® 600 phantom

The CATPHAN® 600 phantom was used to evaluate the image quality of CT system as shown in Figure 3.5. The CATPHAN® phantom is hanging in air at the end of the box placing on the CT table. All test sections can be located by precisely indexing the table from the center of section 1 (CTP404) to the center of each subsequent test module [20]. The indexing distances from first section are listed as follows:

Module	Distance from section 1 center
CTP404, Slice width sensitometry and pixel size	0 mm
CTP591, Bead geometry	32.5 mm
CTP528, 21line pair high resolution	70 mm
CTP528, Point source	80 mm
CTP515, Sub-slice and supra-slice low contrast	110 mm
CTP486, Solid image uniformity module	150 mm

Figure 3.5 CATPHAN® 600 phantom.

3.5.6 Radcal® Accu-gold+

The Radcal® Accu+ gold as illustrated in Figure 3.6 provides a tailored material to diagnostic measurement i.e. radiography, CT, fluoroscopy, mammography and dental equipment. It provides information about dose, dose rate, kV, current (mA), exposure time, half value layer (HVL), waveforms immediately [21].

Figure 3.6 Radcal® Accu-Gold+ digitizer module [21].

3.5.7 CT pencil ionization chamber (10X6-3CT)

CT pencil ionization chamber of 3 cm^3 active volume, 10 cm active length is shown in Figure 3.7. The specification data of CT pencil ionization chamber (10X6-3CT) is shown in Table 3.1. It was designed for CT x-ray beam measurements, either free-in-air or mounted in a head or body phantoms [22].

Figure 3.7 The ionization chamber for measurement of Computed Tomography Dose Index (CTDI) [22].

Table 3.1 Specification data of CT pencil ionization chamber [22].

Title	10X6-3CT	
Min Rate	2μR/s	20 nGy/s
Max Rate	40 R/s	350 mGy/s
Min Dose	20μR	200 nGy
Max Dose	118 kR	1 kGy
Calibration Accuracy	±4% using X-ray @ 150 kVp and 10.2 mm Al HVL	

Title	10X6-3CT
Exposure Rate Dependence	±2%, 2mR/s to 40 R/s
Energy dependence	±5%, 3 to 20 mm Al HVL
Active length / Area	100 mm
Construction	Concentric cylinder. 10 cm active length. 5% uniformity of response over central 95 mm of active length for a constant volume slice. C552 air-equivalent walls and electrode; polyacetal exterior cap; 3 cm^3 active volume; 1.5 m, low noise triax cable; 0.11 kg
Application	CT dose measurement

3.5.8 Syngo CT lung CAD (Computer Aided Detection)

Syngo CT lung CAD was a fully automated computer assisted second reader tool. Syngo CT Lung CAD is designed to assist radiologists in the detection of solid pulmonary nodules during review of CT examinations of the chest. It is intended to be used as a second reader tool after the initial read has been completed [23]. In general, Syngo CT Lung CAD is able to:

- detect round and irregular nodules.
- detect central and peripherally located nodules.
- detect solitary nodules as well as those adjacent to vessels and pleural surfaces.

Figure 3.8 Syngo CT lung CAD algorithm for nodule detection [23].

3.6 Methods

3.6.1 Performance of the dual-source CT (Somatom® Definition Force, Siemens)

The performance of DSCT had been studied according to IAEA Human Health no.19 [24] and CATPHAN® 500 and 600 manual [20]. The program consists of:

- Mechanical accuracy
- Dosimetry CTDI in air and CTDI in phantom
- Image quality performance

3.6.2 Measurement of $CTDI_{air,100}$

The $CTDI_{air,100}$ was measured in all tube potentials for both SE and DE modes in head and body protocols for the accuracy, reproducibility and confidence of using these parameters. The procedures of measurement of $CTDI_{air,100}$ are as followings:

- The CT pencil ionization chamber was placed on the holder at the end of patient table. The ionization chamber was positioned in the air and parallel to the axis of rotation of the scanner.
- Computed Tomography Dose Index in air ($CTDI_{air}$) was measured and recorded by dosimeter reader.
- The scanning parameters were:
  - Head protocols:
    - Single-energy: detector configuration 64 x 0.6 mm with z-flying focal spot and 128 x 0.6 mm with z-flying focal spot, effective mAs of 100, rotation time 1 second, FOV 250 mm, axial mode scan by varying kVp.
    - Dual-energy: detector configuration 64 x 0.6 mm with z- flying focal spot, 128 x 0.6 mm with z-flying focal spot and 192 x 0.6 mm with z-flying focal spot, effective mAs on tube A of 100 and tube B was selected automatically, rotation time 1 second, FOV 250 mm, pitch of 1, helical mode scan by varying kVp.
  - Body protocols:
    - Single-energy: detector configuration 1 x 5 mm and 1 x 10 mm, effective mAs of 100, rotation time 0.5 second, FOV 500 mm, axial mode scan by varying kVp.
    - Dual-energy: detector configuration 64 x 0.6 mm with z- flying focal spot, 128 x 0.6 mm with z-flying focal spot and 192 x 0.6 mm with z-flying focal spot, effective mAs on tube A of 100 and tube B was selected automatically, rotation time 1 second, FOV 500 mm, pitch of 1, helical mode scan by varying kVp.

- $CTDI_{air,100}$ was calculated following equation 2.3 in each kVp in head and body protocols.

3.6.3 Measurement of $CTDI_{vol}$ and Dose Length Product (DLP)

The $CTDI_{vol}$ and DLP were displayed on the console panel of the CT scanner before the scan is initiated. It should be recorded for the accuracy when using these parameters. The procedures of measurement of $CTDI_{vol}$ and DLP are as following:

- The CT pencil ionizing chamber was inserted into the PMMA phantom of 16 and 32 cm in diameter. The position of ionization chamber was at the iso-center of the CT scanner.
- Computed Tomography Dose Index in the phantom were determined and recorded when the chamber was inserted at the center and peripheral hole of the phantom.
- $CTDI_{vol}$ and DLP, displayed on the console panel, were recorded.
- The scanning parameters were:
  - Head protocol: detector configuration 64 x 0.6 mm with z-flying focal spot, effective mAs of 100, rotation time 1 second, FOV 250 mm, axial mode scan by varying kVp in single-energy mode.
  - Body protocol: detector configuration 1 x 10 mm, effective mAs of 100, rotation time 0.5 second, FOV 500 mm, axial mode scan by varying kVp in single-energy mode.
- $CTDI_{vol}$ and DLP of each kVp were calculated following equation 2.4 and 2.5, from the data as shown in the dosimeter, compared to the displayed values on console panel of the CT scanner and compared with the reference dose value from ImPACTscan at the same parameter as the measurement in CTDI in phantom.

3.6.4 Phantom study

Lung man chest phantom was scanned between single- and dual- energy modes. The phantom was attached by five sizes of simulated sphere lesions in the lung field. The locations of simulated lesions were fixed by as following as shown in Figure 3.9.

3 mm in right middle lobe	(green circle)
5 mm in left lower lobe	(yellow circle)
8 mm in right lower lobe	(red circle)
10 mm in left upper lobe	(orange circle)
12 mm in right upper lobe	(pink circle)

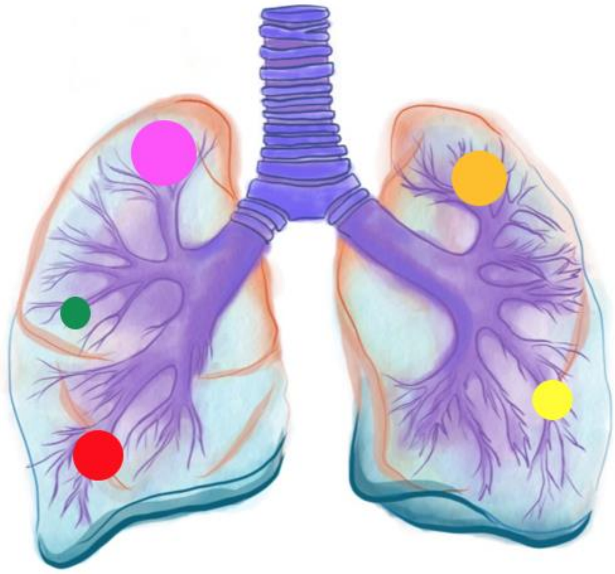

Figure 3.9 The locations of simulated lesions in Lungman chest phantom.

The parameters setting for scan phantom of both energy modes were set as shown in the Table 3.2. All scanning protocols were repeated five times under the same parameter settings.

Table 3.2 Parameter settings in single- and dual- energy modes with various tube potentials.

Parameter	Single-energy mode	Dual-energy mode		
Tube voltage (kVp)	80, 90, 100, 110, 120	80/Sn150,	90/Sn150,	100/Sn150
Tube current time	CAREDose4D	CAREDose4D		
Quality reference mAs	180	180/100*	180/138*	180/100*
Coverage	7th of cervical spine - lower costal margin			
Slice thickness (mm.)	1	1		
Increment (mm.)	0.8	0.8		
Rotation time (s)	0.5	0.28		
Pitch	1.2	0.7		
Detector configuration (mm.)	192 x 0.6**	192 x 0.6**		
DE composition	-	0.7		
Iterative reconstruction	SAFIRE	SAFIRE		

* Quality reference mAs on tube A can adjust to 180 mAs but on tube B were adjusted automatically by CT scanner.

** with z-flying focal spot.

Reference milliampere-seconds (ref mAs.) is a parameter used to specify image quality for CT examinations for reference adults (70 – 80 kg) [25] and performed with a combined modulation type of an automatic exposure-control technique (CareDose 4D, Siemens). Different tube rotation time and pitch were used in single- and dual-energy modes because of the restricted parameter options of the CT scanner.

In dual energy mode, the composite ratio of 0.7 was selected to generate composite image with 30% of information from Sn150-kV and 70% of information from lower energy (80kV, 90 kV, 100kV)

3.6.4.1 Radiation dose evaluated in term of $CTDI_{vol}$, Dose Length Product (DLP) and effective dose.

- **$CTDI_{vol}$ and Dose Length Product (DLP)** were recorded from the CT monitor console panel.
- **Effective dose** was defined as:

$$E = DLP \times K \quad , \tag{3.1}$$

where K denotes conversion factor based on region of body, in this study conversion factor of the chest region equal 0.014 mSv/mGy.cm [10].

3.6.4.2 Image quality characteristics image noise, Contrast to Noise Ratio (CNR) and lesion detectability.

- **Image noise** is defined as the average standard deviation (SD) by drawing region of interest (ROI) at the mediastinum area of the phantom. ROIs size of 4 – 5 cm^2 and equivalent positions in three adjacent slices of the phantom were used for all acquisition protocols as illustrated in Figure 3.10.

Figure 3.10 The measurement of image noise by drawing ROI at the mediastinum area.

- **Contrast to Noise Ratio (CNR)** was determined by drawing two circular ROIs of similar area around the simulated sphere lesion and in the background at the same slice as depicted in Figure 3.11. Each lesion was measured at three adjacent slices from the center of each lesion. ROIs size was approximately 90% of lesion's boundary. The CNR was defined as:

$$CNR = \frac{MPV_{lesion} - MPV_{background}}{\text{Standard Deviation}_{background}} , \qquad (3.2)$$

where MPV_{lesion} and $MPV_{background}$ denote mean pixel value of lesion and background respectively.

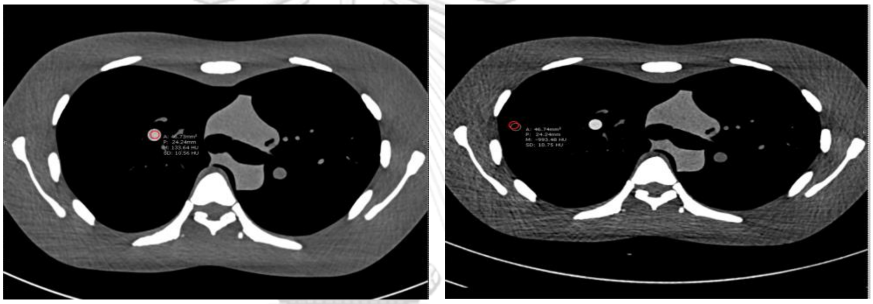

Figure 3.11 Left: ROI of lesion to obtain mean pixel value.
Right: ROI of background to obtain mean pixel value and standard deviation.

The CNR of different parameters in the group were normalized to 120 kVp that as routine setting chest CT protocol. The percent of normalized CNR was defined as:

$$\%CNR = \frac{CNR_i}{CNR_{120\ kVp}} \times 100 , \qquad (3.3)$$

where CNR_i denotes CNR of each acquisition protocol, i denotes 80, 90, 100, 110, 120, 80/Sn150, 90/Sn150, 100/Sn150 kVp respectively.

The percent CNR among the group of the same simulated lesion size were compared at various kVp.

- **Lesion detectability**
  - Using CT lung CAD program to analyze number of simulated lesions in both single- and dual- energy image for lesion detectability.
  - The images were reviewed by three observers in the soft tissue and lung window. They were blinded trial to the parameter techniques. The images were randomly displayed in each observer. The observers scored the lesion detectability by using a five points scale: score 1 means 1 lesion visualized; 2 means 2 lesions visualized; 3 means 3 lesions visualized; 4 means 4 lesions visualized; 5 means 5 lesions visualized.

3.7 Data analysis

$CTDI_{vol}$, DLP, effective dose and the quantitative image quality, image noise and CNR, were determined by using Microsoft excel software to obtain the maximum, minimum, mean, standard deviation values.

The qualitative image quality, lesion detectability, was evaluated by three observers, 1 radiologist and 2 technicians, with similar experience in clinical CT. The five points scales were used to count the simulated nodules as shown in Table 3.3.

Table 3.3 The five points scale for qualitative image quality assessment.

Score	Criteria
5	3, 5, 8, 10, 12 mm in diameter of simulated lesions visualized
4	5, 8, 10, 12 mm in diameter of simulated lesions visualized
3	8, 10, 12 mm in diameter of simulated lesions visualized
2	10, 12 mm in diameter of simulated lesions visualized
1	12 mm in diameter of simulated lesion visualized

3.8 Sample size determination

This is an experimental study. The variable parameters were set. The sizes between two groups are eight values of kVp.

3.9 Statistical analysis

Descriptive statistics; maximum, minimum, mean and standard deviation (SD) by using Microsoft excel software.

3.10 Outcome measurement

Variable: Independent variable = kVp

Dependent variable = Radiation dose, Image noise, CNR, Lesion detectability

3.11 Ethical consideration

This study was performed in the phantom to compare the radiation dose and image quality between single- and dual-energy protocols of chest CT examination. The research proposal has been approved by Ethic committee of Faculty of Medicine, Chulalongkorn University.

3.12 Expected benefit

3.12.1 The patients obtain low radiation dose and sufficient image quality for interpretation of CT radiologist.

3.12.2 Suitable protocol for chest CT examination in dual-energy system for further clinical study are available.

CHAPTER IV
RESULTS

4.1 Quality control of the CT scanner: Siemens dual-source CT

The quality control of CT scanner was performed according to IAEA Human Health Series No.19 and CATPHAN® 500 and 600 manual. The quality control includes the test of mechanical component, radiation dose and image quality performance.

The results of quality control of CT scanner were shown in Appendix B. The summarized reports of CT system performance test were illustrated in Table 4.1.

Table 4.1 Report of CT system performance.

Location:	Bhumisiri Building (2nd floor), King Chulalongkorn Memorial Hospital
Date:	5 May 2017
Room:	CT room
Manufacture:	Siemens Healthcare
M/N and S/N:	Somatom Definition Force M/N: 10414464 and S/N: 614231675

_____Pass____	Scan Localization Light Accuracy
_____Pass____	Alignment of Table to Gantry
_____Pass____	Table Increment Accuracy
_____Pass____	Position Dependence and Signal to Noise Ratio of CT Numbers
_____Pass____	Reproducibility of CT. Numbers
_____Pass____	mAs Linearity
_____Pass____	Linearity of CT. Numbers
_____Pass____	Accuracy of Distance Measurement
_____Pass____	High Contrast Resolution
_____Pass____	Low Contrast Resolution
_____Pass____	Slice Thickness Accuracy (Slide Width)
_____Pass____	Image Uniformity

4.2 Measurement of Computed Tomography Dose Index (CTDI)

4.2.1 CT air kerma index ($CTDI_{air}$)

$CTDI_{air}$ was determined by using 100 mm. pencil ionization chamber placed at the iso-center of the CT gantry. The scan parameters of single- and dual-energy protocols for head and body technique are shown in Table 4.2 and 4.3.

Table 4.2 The scanning parameters of single- and dual-energy for head protocols.

	Single-energy protocols	Dual-energy protocols		
Detector configuration	64 x 0.6 mm.* 128 x 0.6 mm.*	64 x 0.6 mm.* 128 x 0.6 mm.* 192 x 0.6 mm.*		
Tube Potential (kVp)	80, 90, 100, 110, 120, 130, 140, 150, Sn150	80/Sn150	90/Sn150	100/Sn150
Tube-current time (mAs)	100	100/63	100/100	100/63
Mode	Axial scan	Helical scan		
Scan time (second)	1	1		
FOV (mm.)	250	250		
Pitch	-	1		

* with z-flying focal spot.

Table 4.3 The scanning parameters of single- and dual-energy for body protocols.

	Single-energy protocols	Dual-energy protocols		
Detector configuration	1 x 5 mm. 1 x 10 mm.	64 x 0.6 mm.* 128 x 0.6 mm.* 192 x 0.6 mm.*		
Tube Potential (kVp)	80, 90, 100, 110, 120, 130, 140, 150, Sn150	80/Sn150	90/Sn150	100/Sn150
Tube-current time (mAs)	100	100/63	100/100	100/63
Scan time (second)	0.5	1		
FOV (mm.)	500	500		
Mode	Axial scan	Helical scan		
Pitch	-	1		

* with z-flying focal spot.

The results of $CTDI_{air}$ measurement for single- and dual-energy in head phantom are shown as in Table 4.4 and 4.5.

Table 4.4 The measured $CTDI_{air}$ in single-energy for head protocol for each kVp and detector configuration.

	$CTDI_{air}$ (mGy) in head protocol Detector configuration in mm.	
kVp	64 x 0.6	128 x 0.6
80	0.092	0.079
90	0.128	0.109
100	0.167	0.141
110	0.210	0.178
120	0.257	0.218
130	0.306	0.259
140	0.355	0.297
150	0.405	0.346
Sn150	0.087	0.074

$CTDI_{air}$ in single-energy technique using 100 mAs, FOV 250 mm for head technique in each detector configuration were plotted in the Figure 4.1.

Figure 4.1 The relationship between $CTDI_{air}$ and kVp in single-energy among different detector configurations for head protocol were plotted in blue and orange colors of 64 x 0.6 mm and 128 x 0.6 mm respectively.

Table 4.5 The measured $CTDI_{air}$ in dual-energy for head protocol for each kVp and detector configuration.

	$CTDI_{air}$ (mGy) in head protocol Detector configuration in mm.		
kVp	64 x 0.6	128 x 0.6	192 x 0.6
80/Sn150	0.342	0.215	0.173
90/Sn150	0.494	0.310	0.248
100/Sn150	0.514	0.322	0.256

$CTDI_{air}$ in dual-energy technique using 100 mAs on tube A and automatically selected mAs on tube B, FOV 250 mm for head technique in each detector configuration were plotted in the Figure 4.1

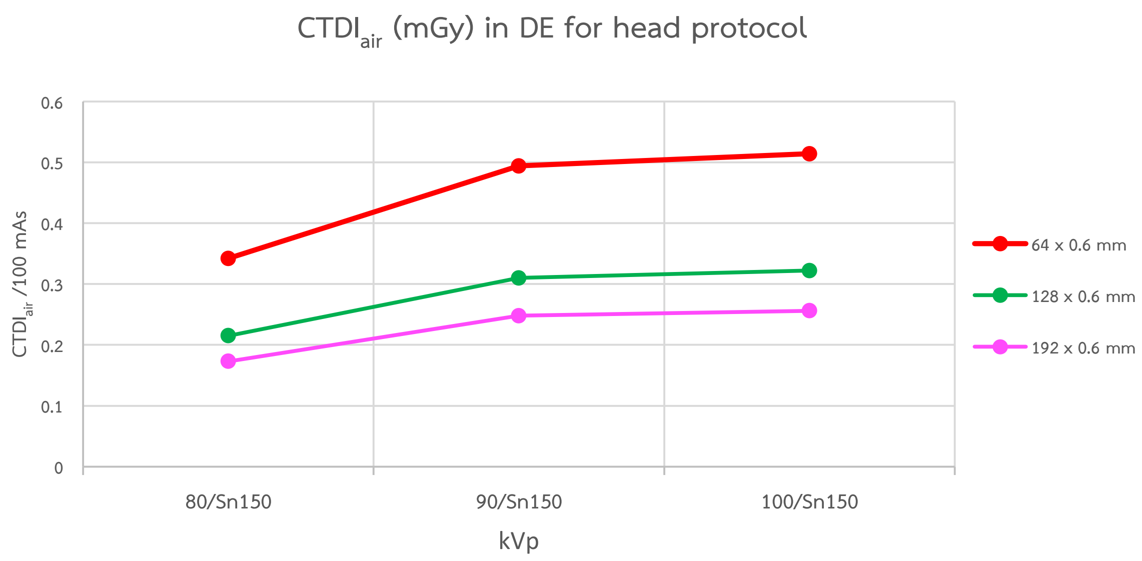

Figure 4.2 The relationship between $CTDI_{air}$ and kVp in dual-energy among different detector configurations for head protocol were plotted in red, green and pink colors of 64 x 0.6 mm, 128 x 0.6 mm and 192 x 0.6 mm respectively.

The results of measured $CTDI_{air}$ for single- and dual-energy in body phantom are shown as in Table 4.6 and 4.7.

Table 4.6 The measured $CTDI_{air}$ in single-energy for body protocol for each kVp and detector configuration.

	$CTDI_{air}$ (mGy) in head protocol Detector configuration in mm.	
kVp	1 x 5	1 x 10
80	0.070	0.070
90	0.128	0.109
100	0.167	0.141
110	0.210	0.178
120	0.257	0.218
130	0.306	0.259
140	0.355	0.297
150	0.405	0.346
Sn150	0.087	0.074

$CTDI_{air}$ in single-energy technique using 100 mAs, FOV 500 mm for body technique in each detector configuration were plotted in the Figure 4.3.

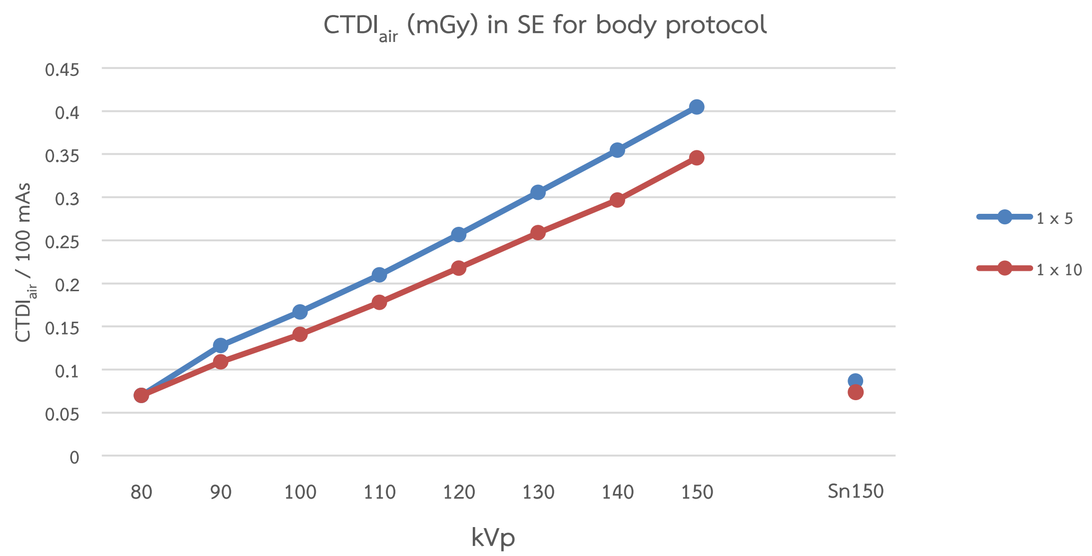

Figure 4.3 The relationship between $CTDI_{air}$ and kVp in single-energy among different detector configurations for body protocol were plotted in blue and red colors of 1 x 5 mm, 1 x 10 mm respectively.

Table 4.7 The measured $CTDI_{air}$ in dual energy for head protocol for each kVp and detector configuration.

	$CTDI_{air}$ (mGy) in head protocol Detector configuration in mm.		
kVp	64 x 0.6	128 x 0.6	192 x 0.6
80/Sn150	0.313	0.196	0.155
90/Sn150	0.420	0.264	0.209
100/Sn150	0.486	0.306	0.227

$CTDI_{air}$ in dual-energy technique using 100 mAs on tube A and automatically selected mAs on tube B, FOV 500 mm for body technique in each detector configuration were plotted in the Figure 4.4.

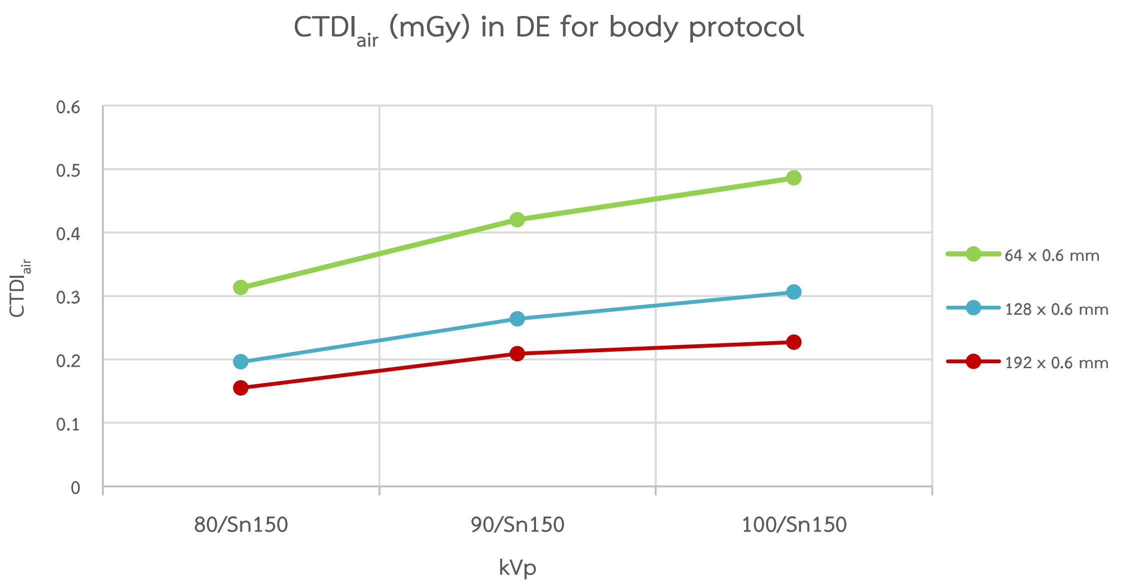

Figure 4.4 The relationship between $CTDI_{air}$ and kVp in dual-energy among different detector configurations for body protocol were plotted in green, blue and red colors of 64 x 0.6 mm, 128 x 0.6 mm and 192 x 0.6 mm respectively.

4.2.2 Weighted CT air kerma Index ($CTDI_w$)

The measured $CTDI_w$ using 100 mm pencil-ionization chamber inserted in each hole, 1 center and 4 peripheries, of 16 cm in diameter of the head phantom and 32 cm in diameter of the body phantom at the iso-center of the CT gantry and the scan parameters were shown in the Table 4.8 and 4.9.

Table 4.8 The scanning parameters of single-energy for head protocol.

Parameters	Single-energy protocols
Detector configuration (mm.)	64 x 0.6 with z-flying focal spot
Tube voltage (kVp)	80, 90, 100, 110, 120, 130, 140, 150, Sn150
Tube – current (mA)	100
Mode	Axial scan
Rotation time (sec)	1
FOV (mm.)	250

Table 4.9 The scanning parameters of single-energy for body protocol.

Parameters	Single-energy protocols
Detector configuration (mm.)	1 x 10
Tube voltage (kVp)	80, 90, 100, 110, 120, 130, 140, 150, Sn150
Mode	Axial scan
Tube – current (mA)	200
Rotation time (sec)	0.5
Effective mAs	100
FOV (mm.)	500

The results of $CTDI_w$ in head and body phantoms are shown as in the Table 4.10 and 4.11 respectively.

Table 4.10 The measured $CTDI_w$ at each hole's position in the head phantom in single-energy protocol for each kVp.

kVp	At center	At the peripheries				$CTDI_w$ (mGy/100mAs)	$_nCTDI_w$ (mGy/mAs)
		3 o'clock	6 o'clock	9 o'clock	12 o'clock		
80	0.979	1.066	0.910	1.038	1.107	5.370	0.054
90	1.440	1.563	1.364	1.525	1.581	7.874	0.079
100	1.956	2.094	1.738	1.978	2.233	10.380	0.104
110	2.524	2.587	2.366	2.543	2.728	13.491	0.135
120	3.161	3.188	2.956	3.286	3.390	16.910	0.169
130	3.842	3.862	3.596	3.979	4.110	20.522	0.205
140	4.504	4.524	4.228	4.663	4.801	24.049	0.240
150	5.173	5.466	4.890	5.379	5.559	27.951	0.280
Sn150	1.201	1.214	1.149	1.192	1.268	6.383	0.064

Table 4.11 The measured $CTDI_w$ at each hole's position in the body phantom in single-energy protocol for each kVp.

kVp	At center	At the peripheries				$CTDI_w$ (mGy/100mAs)	$_nCTDI_w$ (mGy/mAs)
		3 o'clock	6 o'clock	9 o'clock	12 o'clock		
80	0.196	0.433	0.466	0.421	0.429	3.570	0.036
90	0.305	0.636	0.684	0.619	0.632	5.309	0.053
100	0.436	0.872	0.937	0.850	0.869	7.333	0.073
110	0.587	1.145	1.228	1.116	1.135	9.679	0.097
120	0.758	1.448	1.549	1.410	1.435	12.263	0.123
130	0.939	1.759	1.879	1.716	1.744	14.960	0.150
140	1.132	2.097	2.233	2.045	2.078	17.862	0.179
150	1.342	2.456	2.606	2.398	2.436	20.967	0.210
Sn150	0.373	0.616	0.647	0.603	0.612	5.373	0.054

4.2.3 Volume CT Dose Index ($CTDI_{vol}$) on console panel and calculated from $CTDI_w$

The $CTDI_w$ from the Table 4.8 and 4.9 was calculated to obtain $CTDI_{vol}$ for comparison to $CTDI_{vol}$ displayed on console panel, and recorded before the scan. The percent difference between calculated $CTDI_{vol}$ and displayed $CTDI_{vol}$ was shown in the Table 4.12 for $CTDI_{vol}$ in head phantom and Table 4.13 for $CTDI_{vol}$ in body phantom.

Table 4.12 The percent difference between calculated $CTDI_{vol}$ and displayed $CTDI_{vol}$ using head protocol, 100 mAs, 1 second, detector configuration of 64 x 0.6 mm with z-flying focal spot, 250 mm FOV with varying kVp.

kVp	$CTDI_{vol}$ in head phantom (mGy)		% difference
	Calculated	Displayed	
80	5.37	5.50	-3.30
90	7.87	8.08	-2.59
100	10.38	10.95	-5.37
110	13.49	14.11	-4.48
120	16.91	17.59	-3.94
130	20.52	21.17	-3.11
140	24.05	24.94	-3.64
150	27.95	28.91	-3.37
Sn150	6.39	6.66	-4.26

Calculated $CTDI_{vol}$ and displayed $CTDI_{vol}$ using head protocol are plotted in the Figure 4.5.

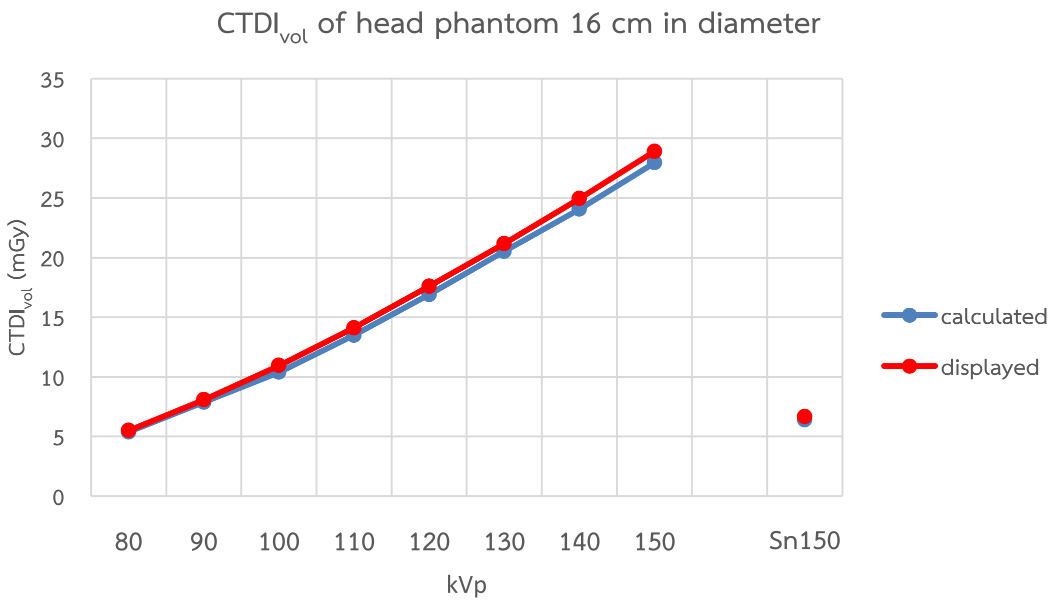

Figure 4.5 The relationship between calculated $CTDI_{vol}$ (blue line) and displayed $CTDI_{vol}$ (red line) of the head phantom in each kVp.

Table 4.13 The percent difference between calculated $CTDI_{vol}$ and displayed $CTDI_{vol}$ using body protocol, 100 mAs, 0.5 second, detector configuration of 1 x 10 mm, 500 mm FOV with varying kVp.

kVp	$CTDI_{vol}$ in body phantom (mGy)		% difference
	Calculated	Displayed	
80	3.57	3.44	3.70
90	5.31	5.15	3.04
100	7.33	7.19	1.97
110	9.68	9.36	3.36
120	12.26	11.92	2.84
130	14.96	14.60	2.44
140	17.86	17.48	2.25
150	20.97	20.50	2.25
Sn150	5.37	5.23	2.70

CTDI$_{vol}$ calculated from CTDI$_{w}$ and CTDI$_{vol}$ displayed on console panel by using body protocol are plotted in the Figure 4.6.

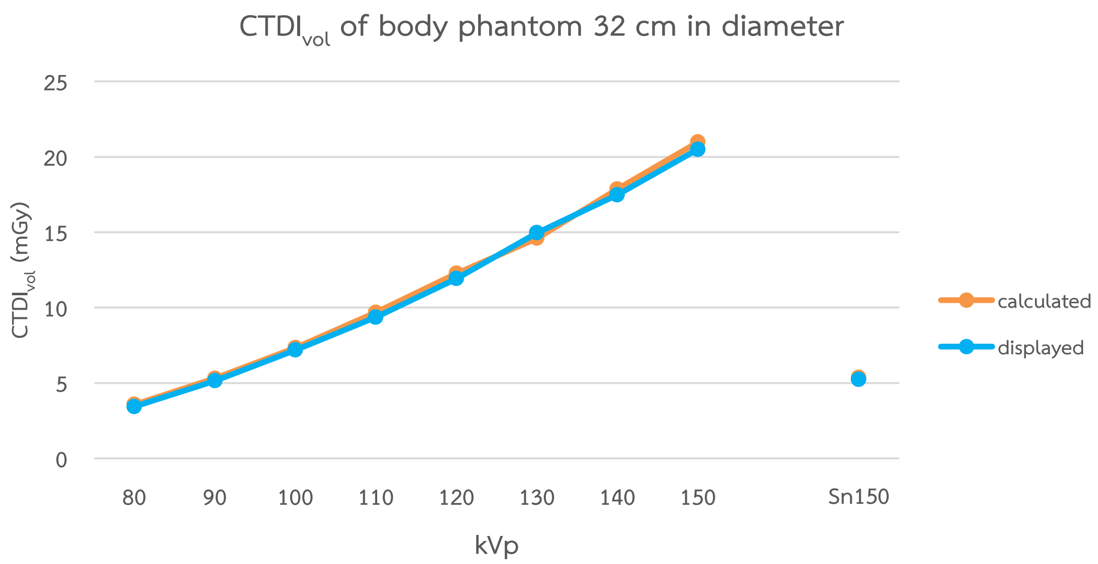

Figure 4.6 The relationship between calculated CTDI$_{vol}$ (orange line) and displayed CTDI$_{vol}$ (blue line) of the body phantom in each kVp.

4.2.4 The displayed and calculated CTDI$_{vol}$ compared with reference CTDI$_{vol}$ values

The displayed CTDI$_{vol}$ and calculated CTDI$_{vol}$ using parameter following as Table 4.8 and 4.9, for head and body protocol respectively, were compared to ImPACT values as illustrated in Table 4.14 and 4.15.

Table 4.14 The displayed and calculated CTDI$_{vol}$ compared to ImPACT using head protocol.

kVp	CTDI$_{vol}$ in head phantom (mGy)		% difference (Calculated and displayed)	ImPACT values	% difference (Calculated and ImPACT)	% difference (displayed and ImPACT)
	Calculated	Displayed				
80	5.37	5.55	-3.30	4.80	11.20	14.49
100	10.38	10.95	-5.37	9.40	9.88	15.23
120	16.90	17.59	-3.94	15.90	6.16	10.09
140	24.05	24.94	-3.64	23.20	3.59	7.23

Table 4.15 The displayed and calculated $CTDI_{vol}$ compared to ImPACT using body protocol.

kVp	$CTDI_{vol}$ in body phantom (mGy) Calculated	$CTDI_{vol}$ in body phantom (mGy) Displayed	% difference (Calculated and displayed)	ImPACT values	% difference (Calculated and ImPACT)	% difference (displayed and ImPACT)
80	3.57	3.44	3.70	3.20	10.92	7.23
100	7.33	7.19	1.97	6.50	12.04	10.08
120	12.26	11.92	2.84	11.20	9.06	6.23
140	17.86	17.48	2.25	16.60	7.32	5.16

4.3 Radiation dose of the phantom

$CTDI_{vol}$ and DLP recorded from console panel of CT scanner on Lungman chest phantom with parameter settings are shown in Table 4.16.

Table 4.16 Parameter setting with scanning Lungman chest phantom.

Parameter	Single-energy mode	Dual-energy mode		
Tube voltage (kVp)	80, 90, 100, 110, 120	80/Sn150,	90/Sn150,	100/Sn150
Tube current time (mAs)	CAREDose4D	CAREDose4D		
Quality reference mAs	180	180/100	180/138	180/100
Coverage	7^{th} of cervical spine - lower costal margin			
Slice thickness (mm.)	1	1		
Increment (mm.)	0.8	0.8		
Rotation time (s)	0.5	0.28		
Pitch	1.2	0.7		
Detector configuration (mm.)	192 x 0.6*	192 x 0.6*		
DE composition	-	0.7		
Iterative reconstruction	SAFIRE	SAFIRE		

* with z-flying focal spot.

The data of mean values of $CTDI_{vol}$ and DLP from scanning five times were shown in the Table 4.17.

Table 4.17 $CTDI_{vol}$ and DLP of Lungman chest phantom in both energy modes.

Tube voltage	$CTDI_{vol}$ (mGy)	DLP (mGy.cm)
80	3.71 $\pm$ 0.30	152.68 $\pm$ 15.67
90	5.07 $\pm$ 0.36	208.94 $\pm$ 19.16
100	6.68 $\pm$ 0.44	275.24 $\pm$ 23.90
110	8.43 $\pm$ 0.50	347.30 $\pm$ 27.78
120	10.44 $\pm$ 0.80	435.42 $\pm$ 33.82
80/Sn150	5.53 $\pm$ 0.24	223.48 $\pm$ 14.74
90/Sn150	7.62 $\pm$ 0.32	307.88 $\pm$ 19.98
100/Sn150	8.17 $\pm$ 0.34	328.70 $\pm$ 21.25

The mean and standard deviation of $CTDI_{vol}$ and DLP of single energy and dual-energy protocols in Lungman chest phantom were plotted against kVp as shown in Figure 4.7 and 4.8 respectively.

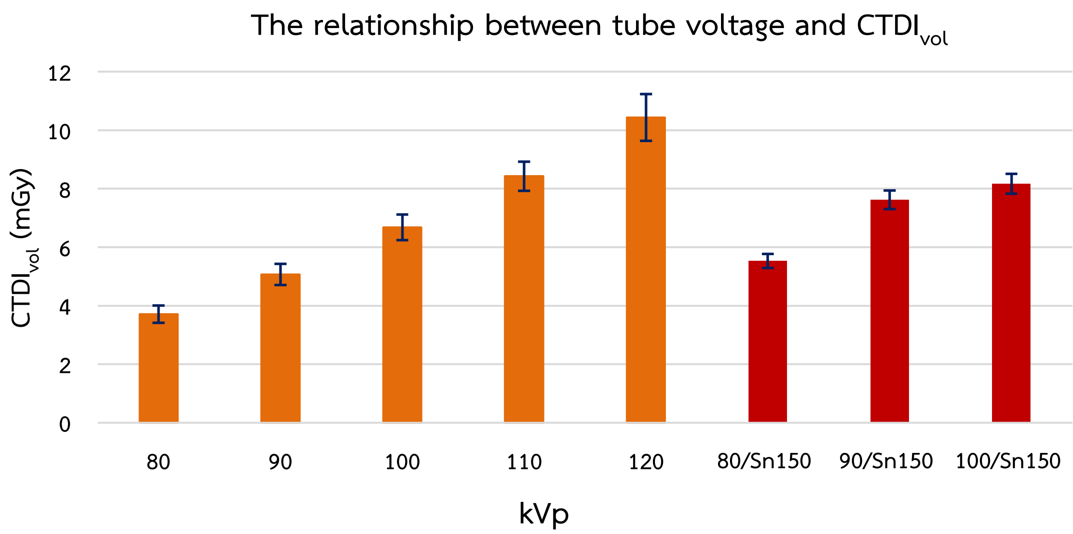

Figure 4.7 The relationship between tube voltage and $CTDI_{vol}$.

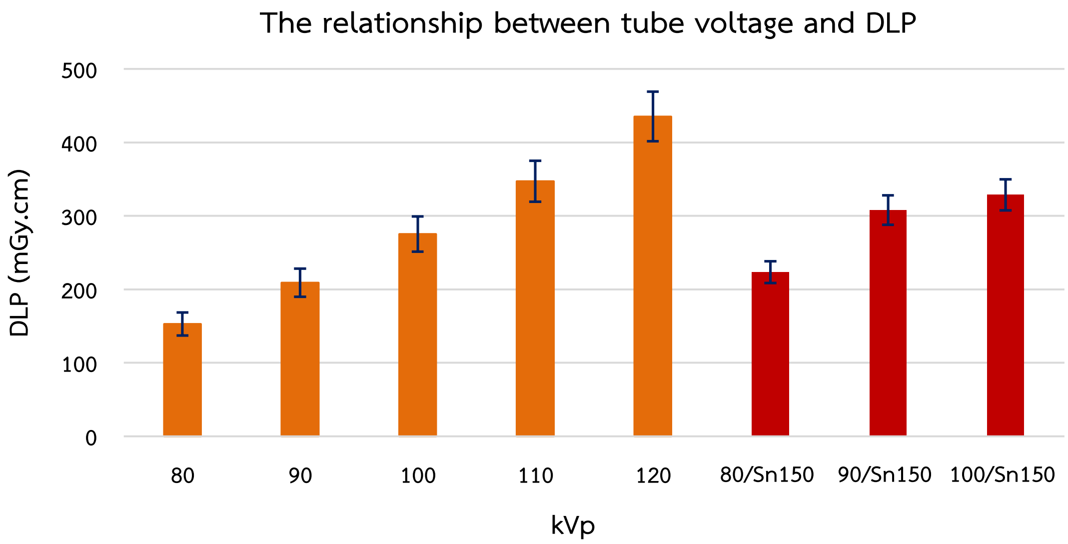

Figure 4.8 The relationship between tube voltage and DLP.

The effective dose is estimated using standard conversion factor 0.014 mSv/mGy.cm for the chest region multiply with DLP as shown in the Table 4.18.

Table 4.18 Estimated effective dose (mSv) from DLP.

Tube voltage	DLP (mGy.cm)	Effective dose (mSv)
80	152.68 ± 15.67	2.14 ± 0.22
90	208.94 ± 19.16	2.93 ± 0.27
100	275.24 ± 23.90	3.85 ± 0.33
110	347.30 ± 27.78	4.86 ± 0.39
120	435.42 ± 33.82	6.10 ± 0.47
80/Sn150	223.48 ± 14.74	3.13 ± 0.21
90/Sn150	307.88 ± 19.98	4.31 ± 0.28
100/Sn150	328.70 ± 21.25	4.60 ± 0.30

The mean values and standard deviation of effective dose in each tube voltage were plotted in Figure 4.9.

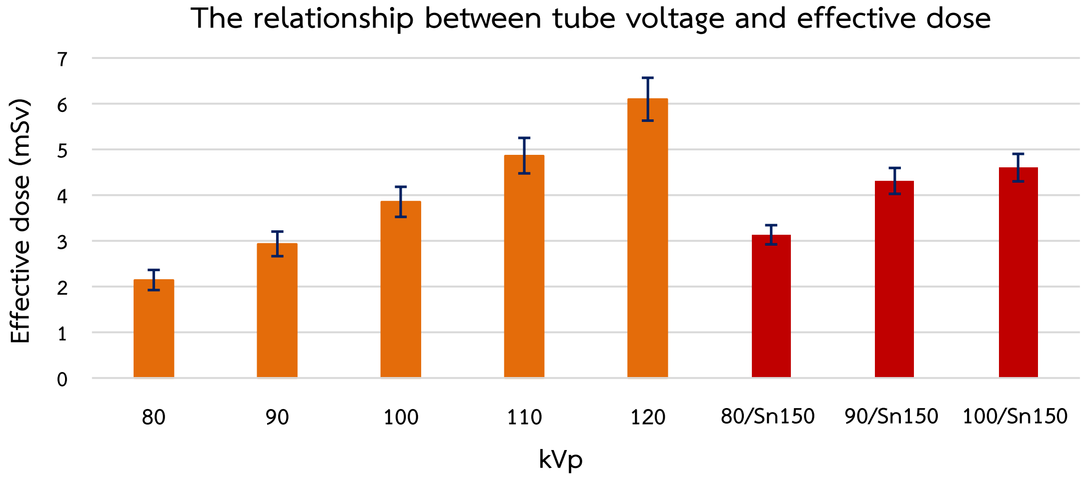

Figure 4.9 The relationship between tube voltage and effective dose.

From the Table 4.18 when increasing kVp in both single- and dual-energy protocols, the radiation dose is increased. In dual-energy protocol results in lower radiation dose than 120 kVp, the highest radiation dose among all protocol. Furthermore, 80 kVp, single-energy protocol, showed the lowest radiation dose.

4.4 Image quality of the phantom

4.4.1 Image noise

The image noise was obtained the standard deviation of CT number, by drawing an ROI at mediastinum of single- and dual-energy composition images. The image noise was shown in the Table 4.19.

Table 4.19 Image noise of single- and dual-energy protocols in Lungman phantom.

Tube voltage	Image noise
80	17.51 ± 2.34
90	13.52 ± 1.79
100	11.24 ± 1.79
110	9.12 ± 0.74
120	8.51 ± 1.23
80/Sn150	13.98 ± 0.82
90/Sn150	10.87 ± 0.37
100/Sn150	9.63 ± 0.69

From Table 4.19 when increasing kVp in both single- and dual-energy protocols, results in decreasing image noise. In dual-energy protocols, the image noise is higher than 120 kVp image, which was lowest image noise among all protocols. The mean values and standard deviation of image noise in each tube voltage were as in Figure 4.10.

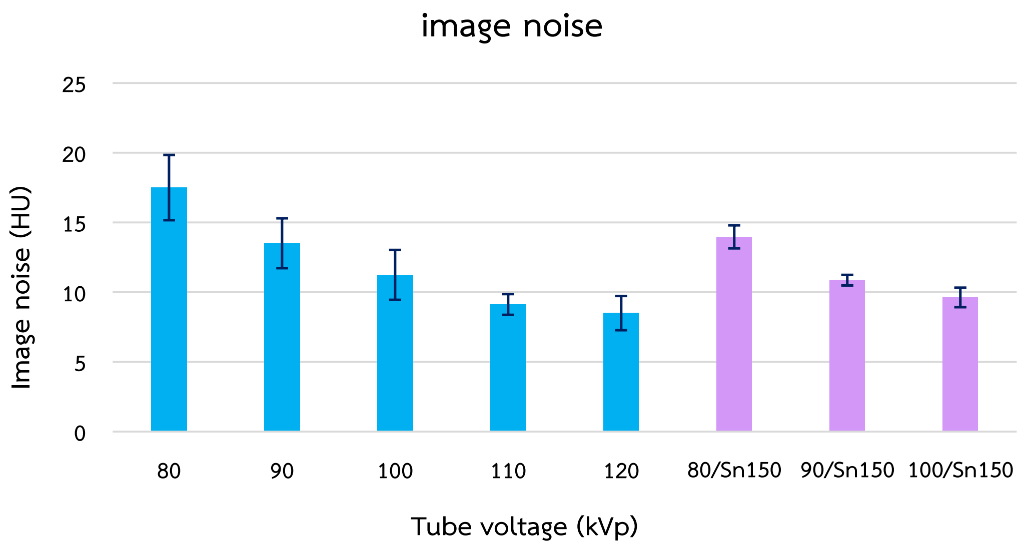

Figure 4.10 The relationship between tube voltage (kVp) and image noise for SE and DE.

4.4.2 Contrast to Noise Ratio (CNR)

CNR was converted to the percent CNR to comparison to the group of the same size of the simulated lesion. The CNR of each kVp was normalized to 120 kVp as routine chest CT protocol as listed in the Table 4.20.

.

Table 4.20 The percent Contrast to Noise Ratio (%CNR) of single- and dual-energy protocols among different lesion diameter.

kVp / size	80	90	100	110	120	80/Sn150	90/Sn150	100/Sn150
3 mm.	41.59	48.73	68.75	89.16	100.00	60.91	78.36	175.35
5 mm.	52.87	70.66	73.52	89.42	100.00	67.95	95.45	109.15
8 mm.	49.87	55.04	77.47	86.03	100.00	69.65	99.67	103.18
10 mm.	44.92	54.54	81.62	96.05	100.00	60.81	78.00	102.07
12 mm.	53.93	66.90	72.65	94.32	100.00	75.18	95.89	116.78

Table 4.20 shows that when increased kVp in both single- and dual- energy protocols, the percent CNR was increasing. The percent CNR at 120 kVp was higher than all SE protocols and DE protocols (80/Sn150 and 90/Sn150 kVp) at all simulated lesions. Conversely, 100/Sn150 kVp offered percent CNR higher than 120 kVp at all simulated lesions.

The percent CNR of all acquisition protocols in each diameter of simulated lesions were plotted as the function tube potentials (kVp) when increasing kVp at the same size of simulated lesion as in Figure 4.11 to 4.15.

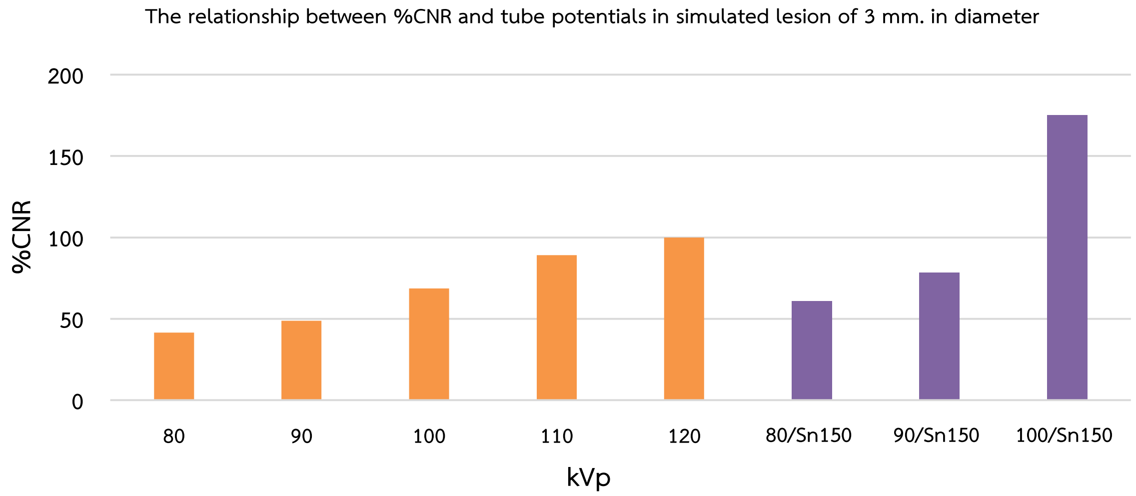

Figure 4.11 The relationship between %CNR and tube potentials in simulated lesion of 3 mm in diameter.

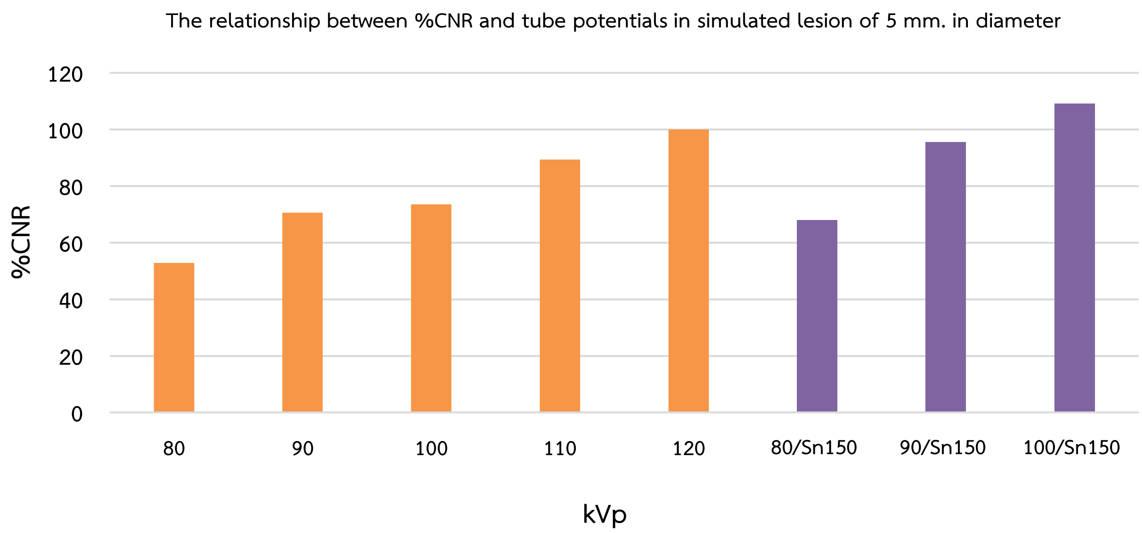

Figure 4.12 The relationship between %CNR and tube potentials in simulated lesion of 5 mm in diameter.

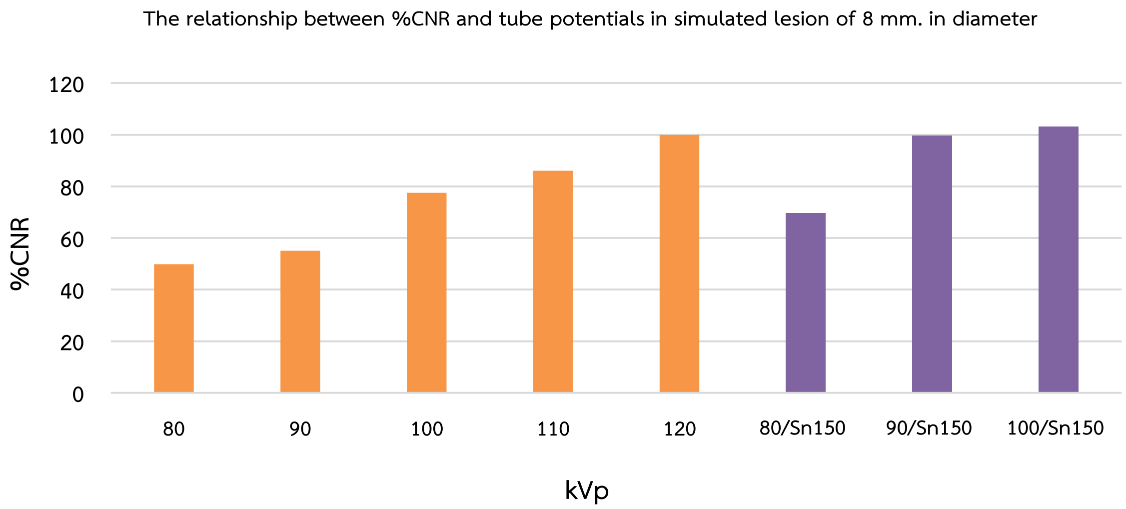

Figure 4.13 The relationship between %CNR and tube potentials in simulated lesion of 8 mm in diameter.

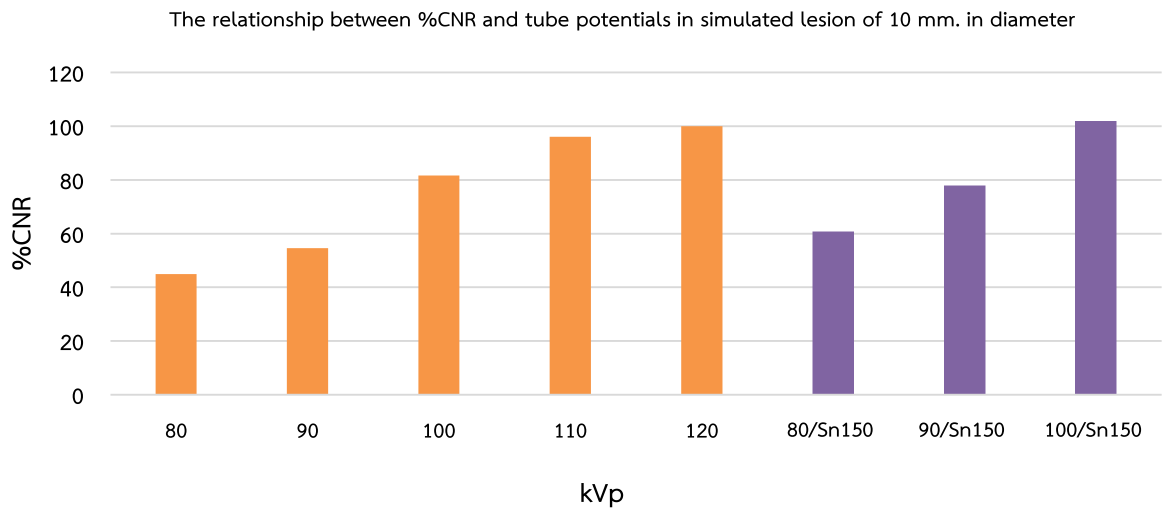

Figure 4.14 The relationship between %CNR and tube potentials in simulated lesion of 10 mm in diameter.

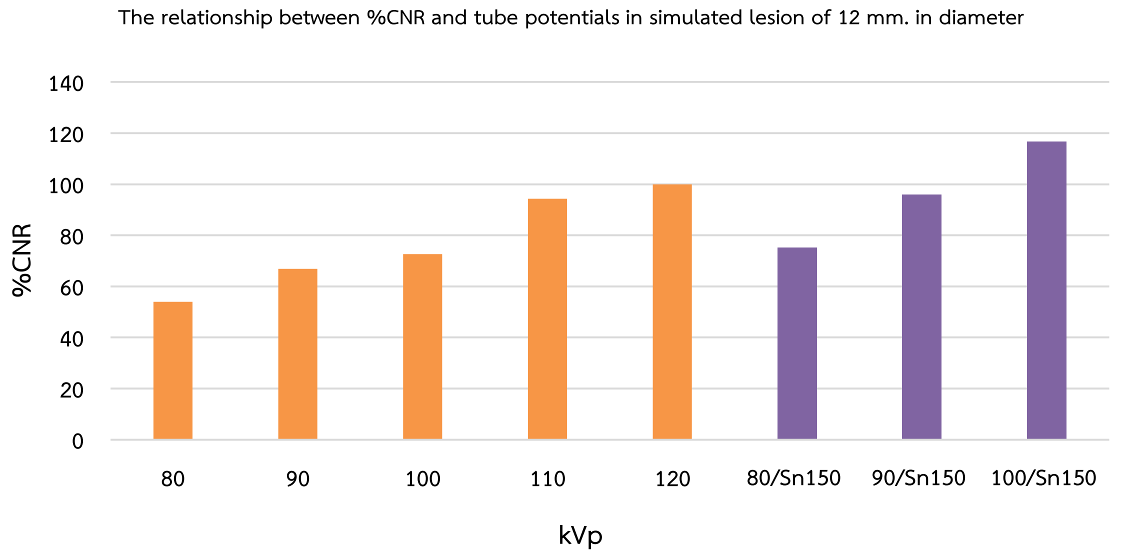

Figure 4.15 The relationship between %CNR and tube potentials in simulated lesion of 12 mm in diameter.

4.4.3 Lesion detectability

- CT lung CAD software:

The images from all acquisition protocol were inputted to the CT lung CAD software. The software can analyze to detect the amount of simulated lesions as listed in the Table 4.21.

Table 4.21 The numbers of simulated lesions detected by the CT lung CAD software.

kVp	Single-energy protocols					Dual-energy protocols		
	80	90	100	110	120	80/Sn150	90/Sn150	100/Sn150
CT lung CAD	5	5	5	5	5	5	5	5

Table 4.21 shows the number of simulated lesions detected by CT lung CAD software of five lesions either single- or dual-energy protocols.

- The Observers:

The images of each acquisition protocol were reviewed by three observers such that they were blinded the parameter settings. The visualization of the number of simulated lesions with varying kVp in the soft tissue window and lung window were listed in the Table 4.22 and 4.23 respectively.

Table 4.22 The numbers of simulated lesions detected by the observers in soft tissue window.

observers \ kVp	Single-energy protocols					Dual-energy protocols		
	80	90	100	110	120	80/Sn150	90/Sn150	100/Sn150
1	4	4	4	4	4	4	4	4
2	4	4	4	4	4	4	4	4
3	4	4	4	5	5	5	5	5

Table 4.23 The numbers of simulated lesions detected by the observers in lung window.

observers \ kVp	Single-energy protocols					Dual-energy protocols		
	80	90	100	110	120	80/Sn150	90/Sn150	100/Sn150
1	5	5	5	5	5	5	5	5
2	5	5	5	5	5	5	5	5
3	5	5	5	5	5	5	5	5

From Table 4.22 and 4.23 show the number of visualized lesions with varying kVp in soft tissue and lung window respectively. For the soft tissue window, the simulated lesions were detected by the observers in dual energy mode as similar to single-energy at 120 kVp. In contrast, in the lung window, all observers can detect more lesions greater than in soft tissue window, results in five lesions detected in both single- and dual- energy protocols.

CHAPTER V
DISCUSSIONS AND CONCLUSIONS

5.1 Discussions

5.1.1 The quality control of CT scanner

The measurement of CTDI and performance of CT scanner are necessary to verify before data collection. The results of CT dose measurements are evaluated for the accuracy and reproducibility. Computed Tomography Dose Index (CTDI) was evaluated following the IAEA Human Health No.19 protocol [24]. The image quality of CT scanner was performed following CATPHAN® 500 and 600 manual [20].

$CTDI_{air,100}$ was measured using pencil ionization chamber in head and body protocols in all kVp both single- and dual-energy techniques. The results of detector configuration (the number of data channels multiplied by the effective detector thickness) were equivalent to beam collimation. $CTDI_{air}$ values decreased when beam collimation increased because the x-ray beam is slightly wider than beam collimation as a result of overbeaming, resulting in a small amount of waste of radiation dose in each rotation. Using small beam collimation contributed to the waste radiation dose at relatively high compared with the primary beam. On the other hand, in larger beam collimation, the waste radiation dose is relatively low compared with the primary beam [26]. Moreover, in each detector configuration when kVp increases in both single- and dual-energy technique, $CTDI_{air}$ increases in both head and body protocols.

For the $CTDI_{vol}$, displayed on control panel, was evaluated and compared with calculated from dosimeter and references dose values from ImPACT at the same kVp, mAs and detector configuration. The difference between calculated $CTDI_{vol}$ and displayed $CTDI_{vol}$ in both head and body protocols was less than 10%. Furthermore, the reference dose values were derived from the ImPACT, the CT machine was used to compare with Somatom Definition AS since Dual source CT isn't available in ImPACT scan. The difference values between reference dose and displayed or calculated $CTDI_{vol}$ in both single- and dual-energy techniques was less than 20%. According to IAEA Human Health No.19 [24], the acceptable value of the difference between displayed and calculated $CTDI_{vol}$ should be less than 20%. The main reason of the difference is the uncertainty in measurement as explain in IAEA Technical Report Series (TRS) No.457: Dosimetry in Diagnostic Radiology: An International Code of Practice [27]. The factor affects to the measurement of CTDI are the characteristic of ionization chamber, the measurement situation, the precision of reading, position of the chamber, the phantom's material composition, the response of the chamber in phantom and the accuracy of laser alignment.

5.1.2 Radiation dose in Lungman chest phantom

The relationship between radiation dose ($CTDI_{vol}$, DLP and effective dose) and kVp in both energy modes show that increasing of kVp result in increasing radiation dose as shown in Table 4.17 and 4.18.

When compare each kVp in single-energy mode at the same quality reference mAs, radiation dose at 120 kVp is highest while 80 kVp is lowest. In addition, when compare each kVp in dual-energy mode, radiation dose of 100/Sn150 kVp is highest whilst 80/Sn150 kVp is lowest. Goldman [11] studied the principle of CT in term of radiation dose and image quality. The results show that increasing kVp is also increasing radiation dose due to increasing intensity of x-ray which penetrated the patient to reach the detector increases.

When compare single- and dual energy modes, the $CTDI_{vol}$, DLP and effective dose values of all dual-energy modes were less than at 120 kVp as similar to Matsubara et al [15]. When CAREDose4D was activated, tube potential of DE (80/Sn140) provided low radiation dose than 120 kVp but the radiation dose at 100/Sn140 was similar to 120 kVp under the same quality reference mAs setting.

5.1.3 Image quality in Lungman chest phantom

5.1.3.1 Image noise

The image noise of single- and dual-energy modes were shown in the Table 4.19. The image noise of dual-energy mode is higher than 120 kVp, lowest among SE protocols, while image noise at 80 kVp was highest as corresponds to radiation dose – radiation dose decreases, image noise will increase as noise is inversely related to the square root of radiation dose [28]. As similar to Schenzle JC [16], the image noise of 120 kVp was lower than dual-energy mode at 100/Sn140 kVp.

5.1.3.2 Contrast to Noise Ratio (CNR)

The CNRs of the simulated lesions of 3, 5, 8, 10 and 12 mm in diameter were classified to groups in order to eliminate of the variance from the location of simulated lesion. At the 120 kVp, baseline set for normalize of CNR as it is usually selected in the clinical chest CT examination. The percent CNR was shown in Table 4.20.

CNR at 80, 90, 100 and 110 kVp were lower than at 120 kVp due to low kVp was more strongly attenuated by iodine than soft tissue but also increase image noise because low-energy of x-ray are absorbed more in soft tissue thus decreasing photons which reaching the detector [29]. Consequently, when Sn150 kVp was selected, CNR will be improved due to radiation dose was higher and the tin (Sn) filter might compensate noise in low tube voltage so that CNR increases. Thus 100/Sn150 kVp offered higher CNR than 120 while 80/Sn150 and 90/Sn150 kVp, CNRs offer lower than 120 kVp because 100 kVp can penetrate the phantom better than 80 and 90 kVp.

Moreover, CT number of simulated lesion 3 mm in all acquisition protocols are lower than CT number designed by manufacturer of this Lungman chest phantom (100 HU) as a result of partial volume effect as imaging voxel containing two different tissues and processing a signal average of both tissues as shown in Figure 5.1.

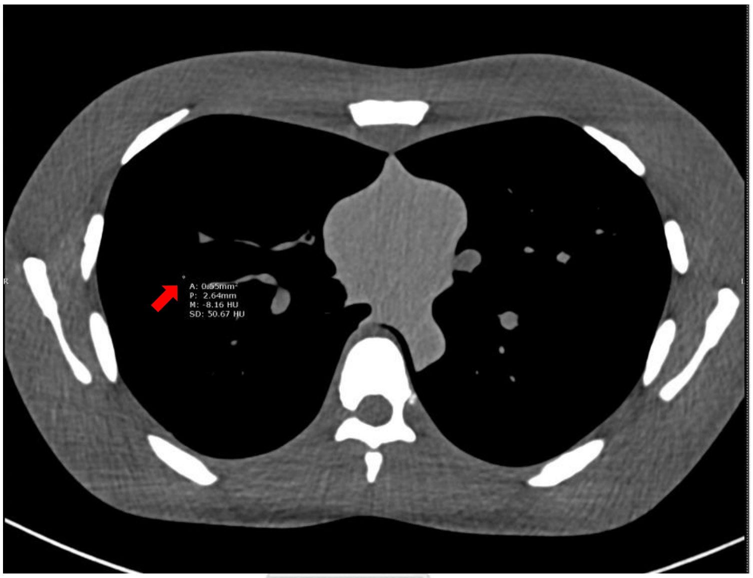

Figure 5.1 Simulated lesion 3 mm in diameter (red arrow) in the soft tissue window at 120 kVp.

5.1.3.3 Lesion detectability

The simulated lesion 3 mm diameter in soft tissue window is difficult to score for lesion detectability by the observers according to the limitation on spatial resolution and partial volume effect.

In addition, the results of the detectability lesion by the observers in soft tissue and lung window were shown in the Table 4.21 and 4.22 respectively. In the lung window, the lesions can be visualized better than soft tissue window in both energy mode because lung window has wider window width and window level (1600 and -600) than soft tissue window (350 and 50) due to wide window width reduce the contrast and detail display, which is suitable for distinguishing the structure with large density difference. Whereas, small window width enhances the contrast and detail display which is suitable for distinguishing the structure with small density difference [30] the lesions can be visualized in lung window in chest clearly than soft tissue window as displayed in Figure 5.2.

Figure 5.2 Simulated lesion 3 mm in diameter (blue arrow) in the lung tissue window at 120 kVp.

When the CT lung CAD software is used to detect the number of simulated lesions in all kVp in both energy modes, five lesions were observed. According to Sahiner et.al [31] studied on the effect of CAD on radiologists' detection of lung nodule in thoracic CT scans, the results from lung CAD was improved thoracic radiologists' performance for detecting pulmonary nodule particularly smaller nodules under 5 mm on CT examinations that may be missed during visual interpretation.

The limitations of this study are as the followings: First, this study was constrained to one size of the Lungman phantom which is standard human size. In small or obese patients, the absorption of x-rays are different thus radiation dose, image noise and CNR might be different. Second, the size and composition of simulated lesions in this study is limited. Third, the investigation was only dual-source CT system (third-generation) and only one quality reference tube-current time setting which usually performed in clinical chest CT protocol at KCMH. Fourth, since the locations of the simulated lesions were fixed in all protocols, the observer can recognize the locations of the simulated lesions, result in the bias in the detection of the lesions. The advantages of DE are mainly used in case of injected contrast media, but our study was performed in phantom without contrast media. However, this study would be beneficial to other studies of dual energy in Thailand.

5.2 Conclusions

DECT offer protocol for lung nodule detection because DECT offers lower radiation dose than SECT (120 kVp), clinical protocol in chest CT examination, in addition to lesion detectability DECT is similar to 120 kVp. In contrast, the image noise of DECT is higher than 120 kVp that affect to interpretation of radiologist. Therefore, DE protocols can be selected under the justification of qualified CT radiologist with the optimal protocol in chest CT examination.

REFERENCES

1. Grajo JR, P.M., Prochowski A, Sahani DV, Dual energy CT in practice: Basic principles and applications. Appl Radiol, 2016. 45(7): p. 6-12.
2. Stolzmann P, L.S., Scheffel H, et al, Characterization of urinary stones with dual energy CT: improved differentiation using a tin filter. Invest Radiol, 2010. 45(1-6).
3. Thieme S, J.T., Lee C, et al, Dual-energy CT for the assessment of contrast material distribution in pulmonary parenchyma. AJR Am J Roentgenol, 2009. 193: p. 144-49.
4. Leng S, Y.L., Fletcher JG, McCollough CH, Maximizing Iodine Contrast-to-Noise Ratios in Abdominal CT Imaging through Use of Energy Domain Noise Reduction and Virtual Monoenergetic Dual-Energy CT. Radiology 2015. 276: p. 562-570.
5. Introduction to solitary pulmonary nodules [online]. 2007 [cited 2017 August 18]; Available from: http://cancergrace.org/lung/2007/11/08/lung-nodule-intro/.
6. Introduction to CT physic [online]. 2004 [cited 2017 August 15]; Available from: http://www.angelfire.com/nd/hussainpassu/Physics_of_Computed_Tomography.pdf.
7. Johnson TR., Dual-energy CT: general principles. AJR Am J Roentgenol, 2012. 199: p. 3-8.
8. ImPACTGroup, Multi-Slice CT scanner CER08007. 2009, Medical Physics Department: Tooting London.
9. Introduction to Computed tomography [online]. 2017 [cited 2017, August 16]; Available from: https://radiologykey.com/computed-tomography-12/.
10. AAPM Report No.96, The measurement, reporting and management of radiation dose in CT. DEFINITIONS OF QUANTITIES FOR ASSESSING DOSE IN CT: CTDI, CTDIFDA, CTDO100, CTDOW, CTDIVOL, DLP, E. 2008. p. 6-13.
11. Goldman LW., Principle of CT: radiation dose and image quality. J Nucl Med Technol, 2007. 35(4): p. 213-25.
12. Romans, LW., Computed tomography for technologists exam review. 2011: Wolters Kluwer Health.
13. Reddinger, W. CT image quality [online]. 1998 [cited 2017 September 17]; Available from: https://www.yumpu.com/en/document/view/2719502/ct-image-quality-wil-reddinger-msc-rtrct
14. SÖderberg M., Automatic exposure control in CT. 2008, Medical Radiation Physics: Lund.
15. Matsubara K, T.T., Kobayashi M, Kobayashi S, Koshida K, Gabata T, Tube Current Modulation Between Single- and Dual-Energy CT with a Second-Generation Dual-Source Scanner: Radiation Dose and Image Quality. American Journal of Roentgenology, 2016. 207(2): p. 354-61.

16. Schenzle JC, S.W., Neumaier K, et al, Dual energy CT of the chest: how about the dose? Invest Radiol, 2010. 45: p. 347-53.
17. Technical specification of Dual-source CT SOMATOM FORCE [online]. [cited 2016 December 19]; Available from: https://www.healthcare.siemens.com/computed-tomography/dual-source-ct/somatom-force/technical-specifications.
18. Multipurpose chest Phantom N1 "LUNGMAN" [online]. [cited 2016 December 19]; Available from: https://www.kyotokagaku.com/products/detail03/pdf/ph-1_catalog.pdf.
19. Radcal-20CT20-Nested-CT-Phantom [online]. 2016 [cited 2017 October 22]; Available from: https://radcal.com/20ct20-nested-ct-head-body-phantom/.
20. Catphan ® 500 and 600 Manual [online]. 2006 [cited 2017 December 22]; Available from: https://static1.squarespace.com/static/5367b059e4b05a1adcd295c2/t/58b5cb7b8419c25b96cba228/1500473967372/Catphan+500600+Manual.pdf.
21. Introduction of Radcal Accu-Gold+ [online]. 2017 [cited 2017 December 22]; Available from: http://radcal.com/rdclwp/wp-content/uploads/2016/11/Radcal-Accu-Gold-Plus-Brochure.pdf.
22. Specification of The Chamber for Computed Tomography Dose Index (CTDI) [online] 2011 [cited 2017 December 22]; Available from: http://radcal.com/rdclwp/wp-content/uploads/2016/10/radcal-10X6-3CT-chamber-spec-sheet.pdf.
23. Overview syngo. CT LungCAD [online]. [cited 2017 December 24]; Available from: https://www.healthcare.siemens.com/computed-tomography/options-upgrades/clinical-applications/ct-syngo-ct-lung-cad.
24. IAEA., Quality Assurance program for Computed Tomography: Diagnostic and therapy Application. IAEA Human Health Serie No.19. 2012, IAEA: Vienna.
25. Introduction of CAREDose4D and Dose Curves [online] 2013 [cited 2017 December 17]; Available from: http://www.dsct.com/index.php/care-dose-4d-and-dose-curves/
26. Siva PR, M.M., Robert VB, Elliot KF, CT Scan Parameters and Radiation Dose: Practical Advice for Radiologists. J Am Coll Radiol, 2013. 10: p. 840-846.
27. International Atomic Energy Agency, Dosimetry in Diagnostic Radiology: An International Code of Practice – Vienna: International Atomic Agency (Technical report reseiers, ISSN 0074-1914; no.457). 2007: Vienna, Austria: IAEA
28. Karmazyn, B., et al., Effect of Tube Voltage on CT Noise Levels in Different Phantom Sizes. American Journal of Roentgenology, 2013. 200(5): p. 1001-1005.
29. Ha HI, H.S., Kim MJ, Lee K, 100 kVp Low-Tube Voltage Abdominal CT in Adults: Radiation Dose Reduction and Image Quality Comparison of 120 kVp Abdominal CT. J Korean Soc Radiol, 2016 Oct. 75(4): p. 285-295.

30. Yao G, Value of window technique in diagnosis of the ground glass opacities in patients with non-small cell pulmonary cancer. Oncol Lett, 2016. 12(5): p. 3993-5.
31. Sahiner B, CHan HP., Hadjiiski LM, Cascade PN, Kazerooni EA, Chughtai AR, et al, Effect of CAD on radiologists' detection of lung nodules on thoracic CT scans: analysis of an observer performance study by nodule size. Acad Radiol, 2009. 16(12): p. 1518-30.

APPENDICES

Appendix A: Data record form

Radiation Dose

Technique	Name of protocol	kVp	C_{vol} (mGy)	DLP (mGy.cm)	Effective dose (mSv)
	1				
	2				
SE	3	80			
	4				
	5				
	1				
	2				
SE	3	90			
	4				
	5				
	1				
	2				
SE	3	100			
	4				
	5				
	1				
	2				
SE	3	110			
	4				
	5				
	1				
	2				
SE	3	120			
	4				
	5				

Radiation Dose (Cont.)

Technique	Name of protocol	kVp	C_{vol} (mGy)	DLP (mGy.cm)	Effective dose (mSv)
DE	1	80/Sn150			
	2				
	3				
	4				
	5				
DE	1	90/Sn150			
	2				
	3				
	4				
	5				
DE	1	100/Sn150			
	2				
	3				
	4				
	5				

<u>CT Number measurement</u>

kVp	Nodule size (mm.)	CT number (nodule)	CT number (background)	S.D. (background)	S.D. (mediastinum)
80	3				
	5				
	8				
	10				
	12				
90	3				
	5				
	8				
	10				
	12				
100	3				
	5				
	8				
	10				
	12				
110	3				
	5				
	8				
	10				
	12				
120	3				
	5				
	8				
	10				
	12				

CT number measurement (Cont.)

kVp	lesion size (mm.)	CT number (lesion)	CT number (background)	S.D. (background)	S.D. (mediastinum)
80/Sn150	3				
	5				
	8				
	10				
	12				
90/Sn150	3				
	5				
	8				
	10				
	12				
100/Sn150	3				
	5				
	8				
	10				
	12				

Lesion Detectability (The observers and CT lungCAD)

Technique	kVp	No. lesion visualized
SE	80	
	90	
	100	
	110	
	120	
DE	80/Sn150	
	90/Sn150	
	100/Sn150	

Appendix B: Quality control of dual-source CT system

1. Scan Localization Light Accuracy

Purpose: To test the congruency of scan localization light and scan plane.

Methods: 1. Tape the ruler on the couch and move couch into the bore was shown in Figure B-1.

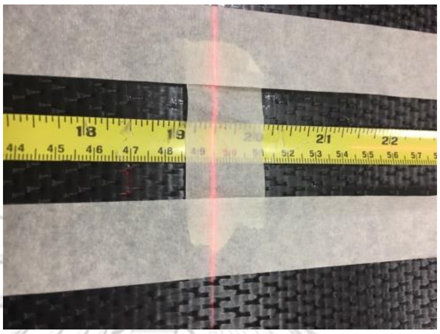

Figure B-1 The measurement of scan localization light accuracy.

2. Mark on the ruler and set zero at the external laser.
3. Move table into the bore.
4. Check internal laser on marker.

<u>Tolerance:</u> Differentiation of the marker between external and internal laser should exceed ± 2 mm.

<u>Results:</u>

External laser:	0.0	cm
Internal laser:	- 0.2	cm
Different:	- 0.2	cm

Comments: Pass

2. Alignment of table to gantry

Purpose: To ensure that long axis of the table is horizontally aligned with a vertical line passing through the rotational axis of the scanner.

Methods:
1. Locate the table midline using a ruler and mark it on a tape affixed to the couch.
2. Extend the table top into gantry to tape position.
3. Measure the horizontal. deviation between the gantry aperture center and the table midline.

Tolerance: The deviation should be less than 5 mm.

Results:

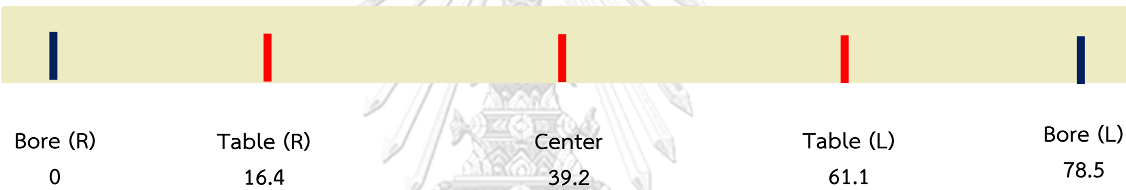

Table B-1: Results of alignment of table to gantry.

	table	Gantry
Distance from right side to center (mm.)	22.80	39.20
Distance from center to left side: (mm.)	21.90	39.30
Measure Deviation* (mm.)	0.45	0.05

$$\text{* Measure deviation} = \frac{\text{(distance from right to center-distance from center to left)}}{2}$$

Comments: Pass

3. Table Increment Accuracy

Purpose: To determine the accuracy and reproducibility of table longitudinal motion.

Method:
1. Tape a measuring tape at the foot end of the table.
2. Set the number of measuring tape to be the center of the tape to function as an indicator.
3. Load table with 70-80 kg, e.g., have assistant lie on table.
4. From the initial position move the table to 300, 400 and 500 mm into the gantry under software control.
5. Record the relative displacement of the pointer the ruler.
6. Reverse the direction of the table and record the value.

Tolerance: Positional error should be less than 3 mm.

Results:

Table B-2: Results of table increment accuracy.

Indicated (mm.)	Measured (mm.)	Deviation* (mm.)
300	300.0	0.0
400	399.9	0.1
500	499.9	0.1
-300	-300.0	0.0
-400	-400.1	0.1
-500	-500.1	0.1

* Deviation = I Indicated – Measured I

Comments: Pass

4. Position Dependence and Signal to Noise Ratio of CT. Numbers

Methods: 1. Position the CT water phantom center in the gantry was shown in Figure B-2.

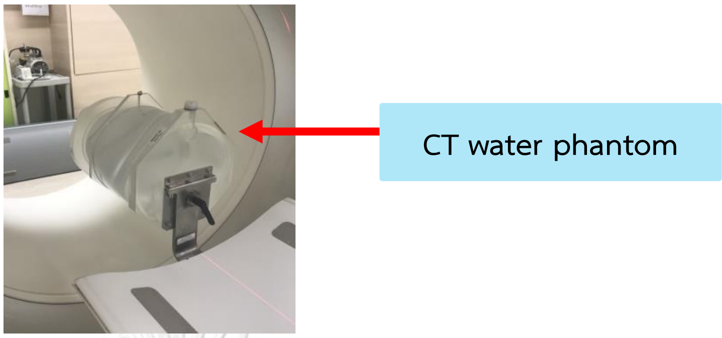

Figure B-2 The position of CT water phantom.

2. Using thickness 10 mm, obtain one scan using typical head technique.
3. The parameters setting are following:
   - Single energy: 120 kVp, 300 mAs, FOV 250 mm.
   - Dual energy: 80/Sn150 kVp, 300/200 mAs, FOV 250 mm.
4. Select a circular ROI of approximately 400 mm^2 and record the mean C.T. number and standard deviation for each of the position 1 to 5 as depicted in Figure B-3.

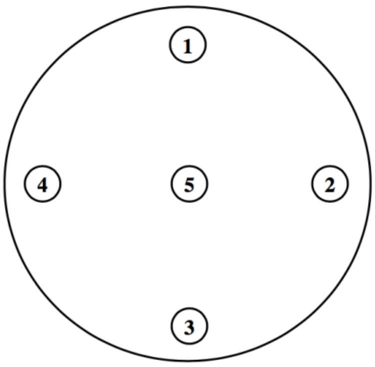

Figure B-3 The position of ROI in CT water phantom images.

Tolerance: The coefficient of variation (COV) should be less than 0.2

Results:

Table B-3: Results of position dependence and S/N ratio of CT number for SE protocol.

Position	Mean C.T.#	S.D.	C.V.	C.O.V.
1	-2.2	2.0	-0.909	-
2	-2.2	1.8	-0.818	0.053
3	-2.2	2.0	0.909	0.053
4	-2.3	2.0	-0.870	0.000
5	-1.2	2.3	-1.917	0.070

Table B-4: Results of position dependence and S/N ratio of CT number for DE protocol.

Position	Mean C.T.#	S.D.	C.V.	C.O.V.
1	1.8	2.8	1.556	-
2	1.3	2.9	2.231	0.018
3	0.8	2.7	3.375	0.036
4	1.1	2.8	2.545	0.018
5	0.2	2.9	14.500	0.018

Comments: Pass

5. Reproducibility of CT. Numbers.

Methods: 1. Using the same set up and parameter setting as position dependence, obtain four scans.
2. Using the same ROI as position dependence in center of the phantom.
3. Obtain mean C.T. numbers for each of the four scans.

Tolerance: The coefficient of variation of mean C.T number should be less than 0.002

Technique: Single energy: 120 kVp, 300 mAs, FOV 250 mm.
Dual energy: 80/Sn150 kVp, 300/200 mAs, FOV 250 mm.

Results:

Table B-5: Results of reproducibility of CT numbers for SE protocol.

Run Number	1	2	3	4
Mean C.T.#	-1.2	-1.1	-0.9	-1.1

Mean Global C.T Number	-1.075
Standard deviation of mean C.T.	0.126
Coefficient of variation	-0.117

Table B-6: Results of reproducibility of CT numbers for DE protocol.

Run Number	1	2	3	4
Mean C.T.#	-0.2	-0.3	-0.1	-0.2

Mean Global C.T Number	-0.200
Standard deviation of mean C.T.	0.082
Coefficient of variation	-0.408

Comments: Pass

6. mAs Linearity

Methods:
1. Set up PMMA head phantom at the center of gantry.
2. Insert 10 cm long pencil chamber in the center slot of the phantom.
3. Select the same kVp and time as used for head scan.
4. Obtain four scans in each of the mA station normally used in the clinic.
5. For each mA, record the exposure in mGy for each scan.
6. Scan should be performed in the increasing order of mA.
7. Compute mGy/mAs for each mA setting.

Technique: 120 kVp, 1.0 sec, FOV 250 mm, varying mA.
Detector configuration 64 x 0.6 mm, with z-flying focal spot.

Results:

Table B-7: Results of mAs linearity for SE protocol.

mA	Exposure in mGy				mGy/mAs	C.V.
	Run 1	Run 2	Run 3	Run 4		
100	3.155	3.152	3.151	3.153	0.030	-
200	6.360	6.362	6.359	6.359	0.030	0.004
300	9.565	9.561	9.562	9.565	0.030	0.001
400	12.770	12.770	12.770	12.770	0.030	0.001
500	15.980	15.970	15.980	15.970	0.030	0.000

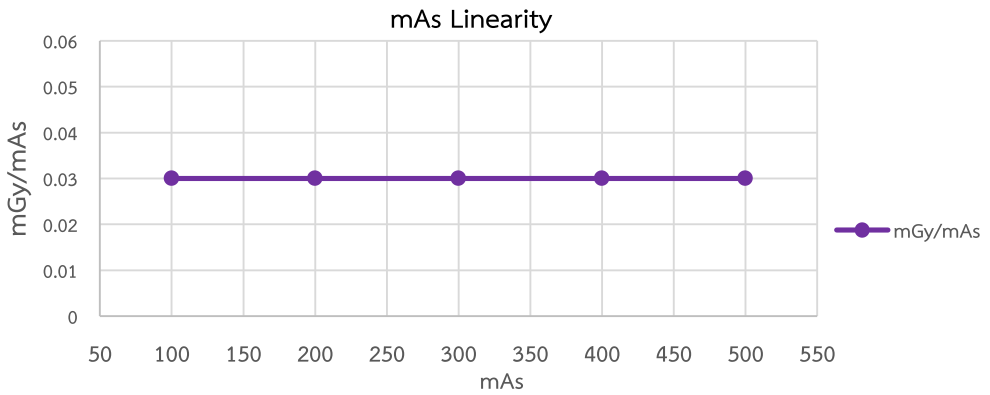

Figure B-4 The relationship between mAs and mGy/mAs.

Comment: Pass

7. Linearity of CT. Numbers

Methods. 1. Set up CATPHAN® 600 phantom as described in beam alignment was shown as Figure B-5.

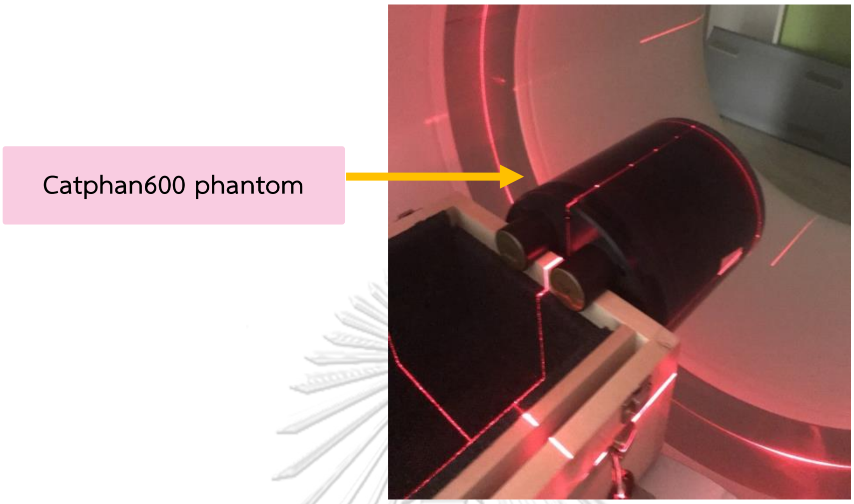

Figure B-5 The position of CATPHAN® 600 phantom.

2. Select the section 1 of the Catphan® 600 phantom which containing the test objects of different C.T numbers (CTP404, sensitometer and pixel size module).
3. Select the head technique and parameter setting as followings:
   - SE (120 kVp), 300 mAs, FOV 250 mm,
     Detector configuration 192 x 0.6 mm, with z-flying focal spot.
     Slice thickness: 1 mm.
   - SE (120 kVp), 300 mAs, FOV 250 mm,
     Detector configuration 48 x 1.2 mm.
     Slice thickness: 2 mm.
   - DE (80/Sn150 kVp), 300/200 mAs, FOV 250 mm,
     Detector configuration, 64 x 0.6 mm, 128 x 0.6 mm, 192 x 0.6 mm, with z-flying focal spot.
     Slice thickness: 1 mm.
4. Draw ROI of sufficient size to cover the test objects and place in middle of each object.
5. Record CT number of each object and record position of table at the center of section 1.

Tolerance: R square value between measured C.T. number and linear attenuation coefficient (μ) more than 0.9

Results:

Table B-8: Results of linearity of CT number for SE protocols at various collimations.

Material	Expected CT number	Measure CT no. SE (192 x 0.6 mm)	Measure CT no. SE (48 x 1.2 mm)	μ(cm^{-1})
Air (Upper)	-1000	-982.56	-982.67	0.000
Air (Lower)	-1000	-984.54	-985.21	0.000
PMP	-200	-181.05	-181.69	0.157
LDPE	-100	-93.12	-93.49	0.174
Polystyrene	-35	-37.85	-36.03	0.188
Acrylic	120	122.02	124.13	0.215
Delrin™	340	330.49	330.88	0.245
Teflon	990	925.18	923.79	0.363

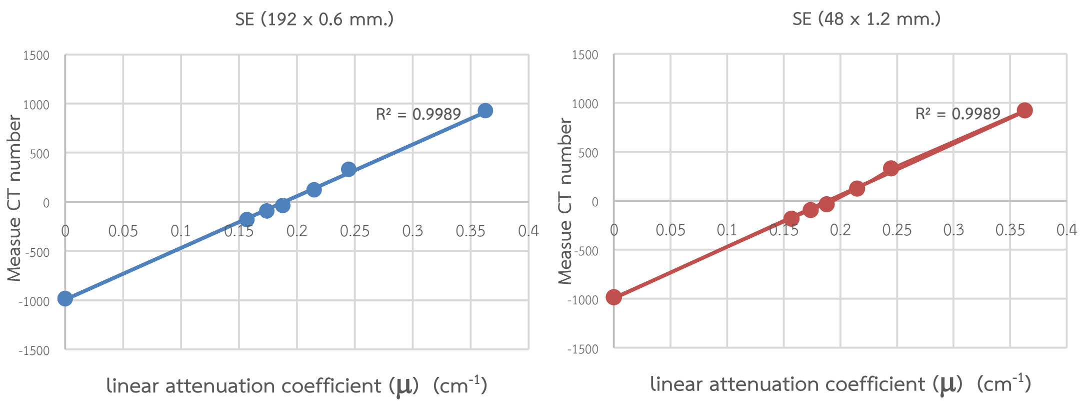

Figure B-6 Left: Linearity of CT number of SE protocol with collimation of 192 x 0.6 mm.
Right: Linearity of CT number of SE protocol with collimation of 48 x 1.2 mm.

Table B-9: Results of linearity of CT number for DE protocols at various collimations.

Material	Expected CT number	Measure CT no. 64x 0.6 mm	Measure CT no. 128 x 0.6 mm	Measure CT no. 192 x 0.6 mm	$\mu(cm^{-1})$
Air (Upper)	-1000	-983.63	-976.35	-975.70	0.000
Air (Lower)	-1000	-984.87	-981.33	-974.76	0.000
PMP	-200	-183.40	-180.31	-180.10	0.157
LDPE	-100	-95.26	-95.07	-93.10	0.174
Polystyrene	-35	-37.03	-36.17	-35.39	0.188
Acrylic	120	118.26	119.33	118.33	0.215
Delrin^{TM}	340	328.12	328.05	328.28	0.245
Teflon	990	920.26	915.13	909.17	0.363

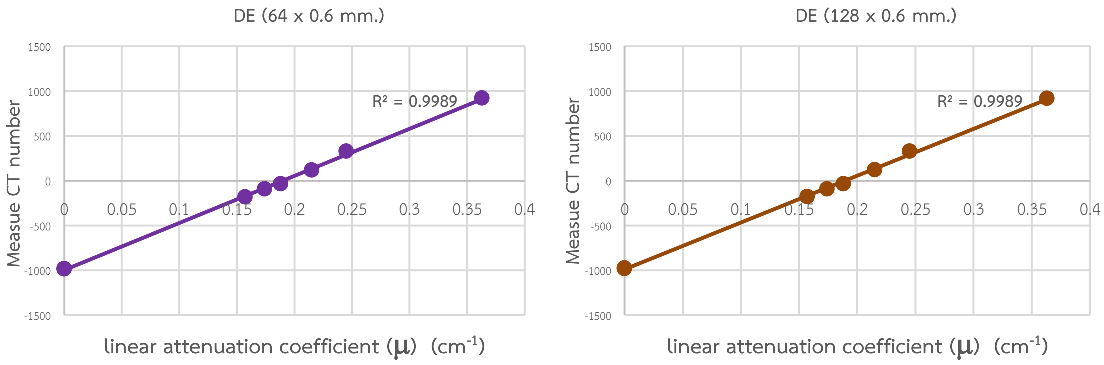

Figure B-7 Left: Linearity of CT number of DE protocol with collimation of 64 x 0.6 mm.
Right: Linearity of CT number of DE protocol with collimation of 128 x 0.6 mm.

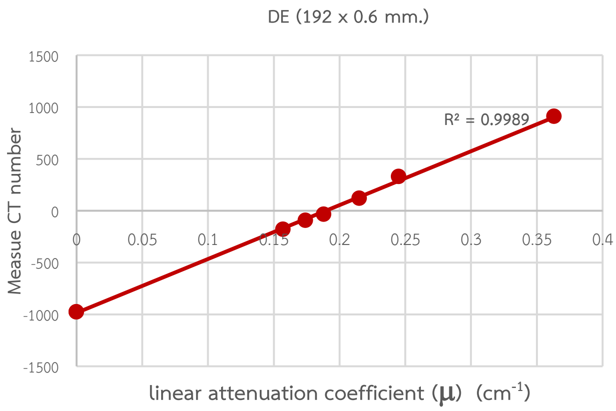

Figure B-8 Linearity of CT number of DE protocol with collimation of 192 x 0.6 mm.

Comments: Pass

8. Accuracy of Distance Measurement

Methods: 1. Set up the CATPHAN®600 phantom as describe in beam alignment.
2. Select the section containing the test accuracy of distance measurement (CTP404, sensitometer and pixel size module).
3. Select head technique and the same parameter setting as linearity of CT number measurement.
4. Measure object in x and y axes was shown in Figure B-9.

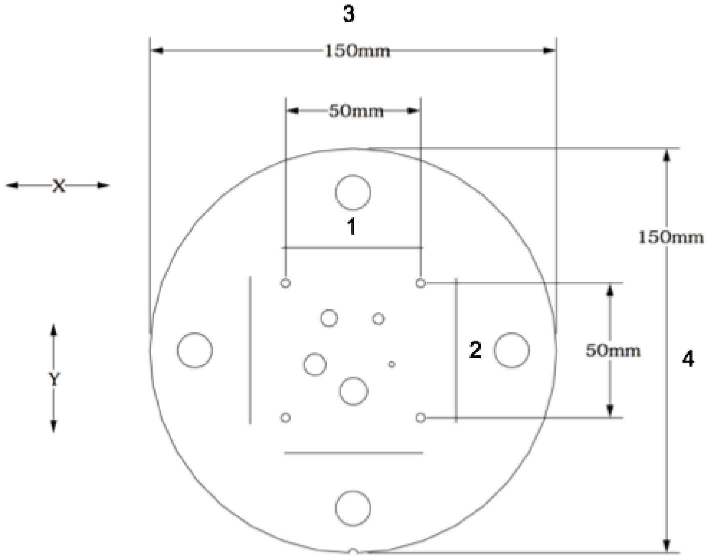

Figure B-9 The measurement of distance accuracy.

Tolerance: Difference between Indicated and measure should be less than 3 mm.

Results:

Table B-10: Results of accuracy of distance measurement for SE protocol with 192 x 0.6 mm detector configuration.

Position	Indicated (mm)	Measured (mm)	Difference (mm)
1	50	50.38	0.38
2	50	50.69	0.69
3	150	150.84	0.84
4	150	150.84	0.84

Difference = I Indicated – Measured I

Table B-11: Results of accuracy of distance measurement for SE protocol with 48 x 1.2 mm detector configuration.

Position	Indicated (mm)	Measured (mm)	Difference (mm)
1	50	50.38	0.38
2	50	50.23	0.23
3	150	150.69	0.69
4	150	150.99	0.99

Table B-12: Results of accuracy of distance measurement for DE protocol with 64 x 0.6 mm detector configuration.

Position	Indicated (mm)	Measured (mm)	Difference (mm)
1	50	49.77	0.23
2	50	50.69	0.69
3	150	150.84	0.84
4	150	150.53	0.53

Table B-13: Results of accuracy of distance measurement for DE protocol with 128 x 0.6 mm detector configuration.

Position	Indicated (mm)	Measured (mm)	Difference (mm)
1	50	50.08	0.08
2	50	50.23	0.23
3	150	150.23	0.23
4	150	150.69	0.69

Table B-14: Results of accuracy of distance measurement for DE protocol with 192 x 0.6 mm detector configuration.

Position	Indicated (mm)	Measured (mm)	Difference (mm)
1	50	50.23	0.23
2	50	50.69	0.69
3	150	150.07	0.07
4	150	150.53	0.53

Comments: Pass

9. High Contrast Resolution

Methods: 1. Set up CATPHAN® 600 phantom as described in beam alignment.

2. Select the section of Catphan600 phantom which containing the high contrast resolution test object. (CTP528, 21line pair high resolution, distance) was shown in Figure B-10.

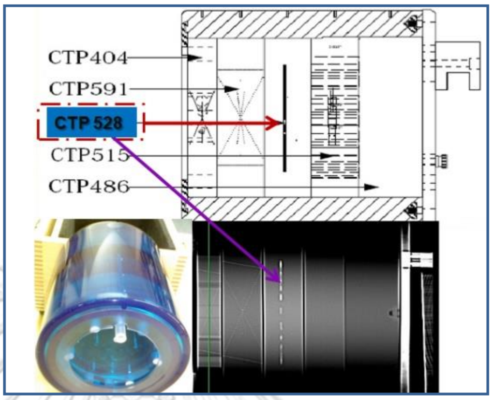

Figure B-10 The module of high contrast resolution test object.

3. Select the head technique and the same parameter setting as linearity of CT number measurement.
4. Select the area containing the high contrast resolution test objects and adjust appropriate window and level for the best visualization of the test objects and magnify as necessary.
5. Record the smallest test object visualized on the monitor.

Tolerance: Should be more than 5-line pairs/cm

Results:

Table B-15: Results of high contrast resolution for SE protocols with various collimations.

Techniques	Resolution
SE (120 kVp), Detector configuration 192 x 0.6 mm	6 (0.083 cm)
SE (120 kVp), Detector configuration 48 x 1.2 mm	6 (0.083 cm)

Table B-16: Results of high contrast resolution for DE protocols with various collimations.

Techniques	Resolution
DE (80/Sn150 kVp), Detector configuration 64 x 0.6 mm	6 (0.083 cm)
DE (80/Sn150 kVp), Detector configuration 128 x 0.6 mm	6 (0.083 cm)
DE (80/Sn150 kVp), Detector configuration 192 x 0.6 mm	7 (0.071 cm)

Comments: Pass

10. Low contrast Resolution

Methods: 1. Set up the CATPHAN® 600 phantom as described in beam alignment.

2. Select the head technique and the same parameter setting as linearity of CT number measurement.

3. Select the section containing the low contrast resolution test object. (CTP515, sub-slice and supra-slice low contrast.) was shown in Figure B-11.

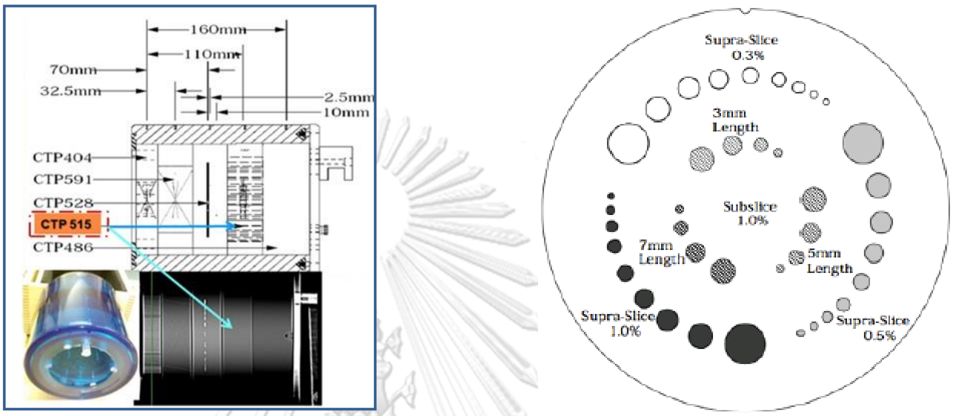

Figure B-11 The module of low contrast resolution test object.

4. Select appropriate window and level for the best visualization of the test objects.

5. Record the smallest test object visualized.

Tolerance: The smallest diameter hole 7 mm (4 holes) should be seen at 0.5% contrast

Results:

Table B-17: Results of low contrast resolution for SE protocols with various collimations.

	Nominal target contrast level	No. spokes Detector configuration 192 x 0.6 mm	No. spokes Detector configuration 48 x 1.2 mm
Supra-slice	0.3 %	1	1
	0.5 %	4	6
	1.0 %	7	8
Sub-slice	3 mm length	4	3
	5 mm Length	4	3
	7 mm Length	4	4

Table B-18: Results of low contrast resolution for DE protocols with various collimations.

	Nominal target contrast level	No. spokes Detector configuration 64 x 0.6 mm	No. spokes Detector configuration 128 x 0.6 mm	No. spokes Detector configuration 192 x 0.6 mm
Supra-slice	0.3 %	1	1	1
	0.5 %	4	4	4
	1.0 %	6	7	6
Sub-slice	3 mm length	3	2	2
	5 mm Length	3	3	2
	7 mm Length	3	2	3

Comments: **Pass**

11. Slice Thickness Accuracy (Slice Width)

Methods: 1. Set up the CATPHAN®600 phantom as described in beam alignment.

2. Select the section1 which have wire ramps are used to estimate slice width measurements (CTP404, sensitometer and pixel size module).
3. Select the head technique and the same parameter setting as linearity of CT number measurement
4. Perform several scans with different slice thickness under the same parameter.
5. Calculate the real slice width following Catphan manual in each slice collimation as:
   i. Draw ROI to identify mean CT number of the area adjacent to the wire ramp for define as "Background"
   ii. Adjust window width to 1
   iii. Move window level to the point where the wire ramp disappear.
   iv. Determine window level at this position is "Maximum value"
   v. Define the half maximum CT by:
      a. Net peak CT = Maximum value – Background
      b. 50% Net peak CT = $\frac{\text{Net peak CT}}{2}$
      c. Half maximum CT = 50% Net peak CT + Background
   vi. Adjust window level to be equal at half maximum CT.
   vii. Draw line along the ramp that show length of each ramp.
   viii. Average length of 4 wire ramp as FWHM.
   ix. Slice width = FWHM x 0.42

Tolerance: The deviation should be less than 1 mm.

Results:

Table B-19: Results of slice thickness accuracy for SE and DE protocols with various collimations.

Technique (kVp)	Detector configuration (mm)	Slice thickness (mm)	Measure thickness (mm)	Deviation* (mm)
SE (120 kVp)	192 x 0.6	1	1.28	0.28
	48 x 1.2	2	2.14	0.14
DE (80/Sn150 kVp)	64 x 0.6	1	1.26	0.26
	128 x 0.6	1	1.27	0.27
	48 x 0.6	1	1.27	0.27

* Deviation = I Slice thickness – Measure thickness I

Comments: Pass

12. Image Uniformity

Methods:

1. Set up the CATPHAN®600 phantom as described in beam alignment.
2. Select the section6 (CTP 486, Solid image uniformity module) used to estimate image uniformity.
3. Select the head technique and the same parameter setting as linearity of CT number measurement.
4. Draw ROI of approximately 400 mm^2 and place in the middle and peripheral of the phantom in each slice thickness as illustrated in Figure B-12.

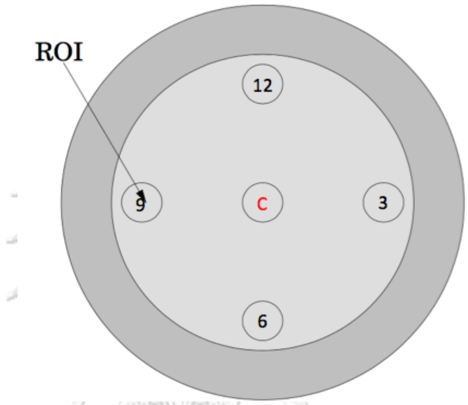

Figure B-12 The measurement of image uniformity.

5. Record the mean C.T number of middle and peripheral of the phantom.

Tolerance: Difference should be less than 5 HU.

Results:

Table B-20: Results of image uniformity for SE (120 kVp) with 192 x 0.6 mm detector configuration.

position	Mean C.T.#	S.D.	Different of C.T. no.
Center	7.04	4.75	0.00
3 o'clock	7.40	4.06	0.36
6 o'clock	7.47	4.42	0.43
9 o'clock	7.45	4.61	0.41
12 o'clock	7.03	4.30	0.01

Different of C.T. Number = I Mean C.T number at center – Mean C.T. number at peripheral I

Table B-21: Results of image uniformity for SE (120 kVp) with 48 x 1.2 mm detector configuration.

position	Mean C.T.#	S.D.	Different of C.T. no.
Center	7.42	3.77	0.00
3 o'clock	7.26	3.30	0.16
6 o'clock	7.75	3.23	0.33
9 o'clock	7.34	3.14	0.08
12 o'clock	7.37	2.75	0.05

Table B-22: Results of image uniformity for DE (80/Sn150 kVp) with 64 x 0.6 mm detector configuration.

position	Mean C.T.#	S.D.	Different of C.T. no.
Center	5.73	8.59	0.00
3 o'clock	6.94	6.73	1.21
6 o'clock	6.74	7.61	1.01
9 o'clock	7.58	6.70	1.85
12 o'clock	7.24	6.71	1.51

Table B-23: Results of image uniformity for DE (80/Sn150 kVp) with 128 x 0.6 mm detector configuration.

position	Mean C.T.#	S.D.	Different of C.T. no.
Center	5.9	8.57	0.00
3 o'clock	7.18	6.99	1.28
6 o'clock	7.24	6.95	1.34
9 o'clock	6.87	7.26	0.97
12 o'clock	6.93	7.12	1.03

Table B-24: Results of image uniformity for DE (80/Sn150 kVp) with 192 x 0.6 mm detector configuration.

position	Mean C.T.#	S.D.	Different of C.T. no.
Center	6.21	7.96	0.00
3 o'clock	6.51	7.18	0.30
6 o'clock	7.12	7.03	0.91
9 o'clock	6.83	7.08	0.62
12 o'clock	6.39	6.53	0.18

Comments: Pass

VITA

NAME: Mr. Taninchai Jutawiriya

DATE OF BIRTH: 8 June 1990

PLACE OF BIRTH: Nakhonratchasima, Thailand

EDUCATION: Bachelor of Science (Radological Technology)
Faculty of Medical Technology,
Mahidol University, 2012

ADDRESS: 890/260 Lumipini park Rama9-Ratchada
Chaturathi rd. Huai Khwang, Bangkok 10310,
Thailand.

E-MAIL: Taninchai.j@hotmail.com

ACADEMIC PUBLICATION:

1. Jutawiriya T., Krisanachinda A. Radiation Dose and Image Quality in Chest Region Using Single- and Dual-Energy CT; Phantom Study. In Proceedings of 15th South East Asian Congress of Medical Physic, pp. 107-112, Philippines, 2017

2. Jutawiriya T., Krisanachinda A. Comparison Between Single- and Dual-Energy CT in Chest Phantom: Radiation Dose and Image Quality. In Proceedings of 10th Annual Scientific Meeting of Thai Medical Physicist Society (TMPS), pp. 96-99, Bangkok, Thailand, 2018.